Universitetet
i Stavanger

Faculty of Science and Technology

MASTER'S THESIS

Study program/specialization: Biological chemistry	Spring semester, 2019 Open access
Author: Saleha Akbari	Saleha Akbari (Author's signature)
Supervisor: Astrid Elisabeth Mork-Jansson	
Title of thesis: Isolation and characterization of exosomes from human plasma related to development of a nanocarrier for epilepsy treatment	
Credits: 60	
Key words: Exosomes, dynamic light scattering, blood-brain barrier, nano-carrier, characterization, size exclusion chromatography, plasma, western blotting, internalization and drug delivery system.	Pages: 64 + Appendices: 68 Stavanger, 14 June-2019

Title page for Master's Thesis
Faculty of Science and Technology

University of Stavanger – Faculty of Science and technology

Master's Thesis

Biological Chemistry Master's Program

Isolation and Characterization of Exosomes from Human Plasma Related to Development of a Nanocarrier for Epilepsy treatment

Supervisor: Astrid Elisabeth Mork-Jansson

Saleha Akbari

219804

s.akbari@uis.no

June 2019

Abstract

The investigation of exosomes as a cell-mediated delivery system for the delivery of nucleic acids, proteins and low molecular-weight therapeutic drugs increased during the past two decades. The potential of exosomes as drug delivery vesicles has enticed a significant attention due to the elucidation of their advantages and the impressive capacity they have. Here, exosomes were characterized, standard preservation determined and internalization of exosomes to human cerebral microvascular endothelial cells investigated.

In this project, vesicles from human plasma were isolated by size exclusion chromatography. Isolated vesicles were characterized as exosomes by applying different methods prior to further experiments. Vesicles in the size-range 30 -100 nm were indicated in dynamic light scattering measurements, which was the expected size for exosomes. The exosome protein marker, HSP70 was detected in the western blotting. Furthermore, the labeled exosomes were visualized by a laser scanning confocal microscopy.

The characterization of isolated vesicles by dynamic light scattering showed homogenous fractions of vesicles. The downstream identification of HSP70, suggested that the isolated vesicles might be indeed exosomes. Dynamic light scattering measurements and measuring absorbance of lipids and proteins present in exosomes suggested that the size, homogeneity and the total content of exosomes were preserved better at room temperature and 4°C than storage at - 80°C and - 20°C.

The successful characterization of isolated vesicles allowed exosomes uptake assays to be analyzed by confocal microscopy. Pre-stained exosomes were integrated into a human cerebral microvascular endothelial cell line as a model for the human blood-brain barrier, and internalization of exosomes into the cells was assessed by confocal microscopy. The results suggested possible uptake of exosomes into human cerebral microvascular endothelial cells. However, the exact localization of exosomes in the cells remained unclear.

Acknowledgements

In the name of Allah, the Creature of the whole existence which the knowledge of mankind are unable to grip the greatness of his creaturely. Firstly, I would like to take this opportunity to thank my dear parents to their affection during all my life. They who supported my education despite all restrains and challenges they had.

This thesis was a part of the project proposed by Astrid Elisabeth Mork-Jansson, and the practical works were performed at the laboratory in Centre for Organelle Research (Core). The work was carried out under the supervision of Astrid Elisabeth M-Jansson at the University of Stavanger in 2018 – 2019.

I would like to thank my main supervisor Astrid Elisabeth M-Jansson for all her guidance and advice throughout this thesis. I would also like to thank Julie Nikolaisen for her help and supplying compounds required during laboratory works. Thanks also to Jodi Maple Grødem who performed training on confocal microscopy, helped us with analysis of the confocal microscopy images and last prat of writing.

Special thanks to my husband Gholam Sakhi Sakha for his supporting and my darlings Melika and Mobina for their loves and their apperception in my absence. Thank finally to my fellow students, Susanne Nesse and Azam Daraei for their advice and discussions regarding this thesis.

Saleha Akbari
June 2019

Table of Contents

List of Abbreviations

AB	Apoptotic body
ABC	Adenosine triphosphate-binding cassette
ACF	Autocorrelation factor
AD	Alzheimer's disease
AED	Antiepileptic drug
AJ	Adherence junction
AMT	Adsorptive-mediated transcytosis
ATP	Adenosine triphosphate
BBB	Blood brain barrier
BCA	Bicinchoninic acid
bEND.3	brain endothelial cell line
BL	Basal lamina
BSA	Bovine serum albumin
CNS	Central nerve system
CBZ	Carbamazepine
CBB	Coomassie brilliant blue
D	Dimension
DAPI	4',6-diamidino-2-phenylindole
CD	Cluster of differentiation
CLS	Capillary-like structure
Core	Centre for Organelle Research
DLS	Dynamic light scattering
DMSO	Dimethyl sulfoxide
DNA	Deoxyribonucleic acid
Dox	Doxorubicin
ECL	Enhanced chemiluminescence
EGF	Epidermal growth factor
Em	Emission
EV	Extracellular vesicle
Ex	Excitation
FBS	Fetal bovine serum

FGF	Fibroblast growth factor
GAPDH	glyceraldehyde-3-phosphate dehydrogenase
GJs	Gap junctions
HBSS	Hank's balanced salt solution
hCMEC/D3	human cerebral microvascular endothelial cells
HSP	Heat shock protein
HRP	Horseradish peroxide
IAC	Immunoaffinity capture
JAM	Junctional adhesion molecule
LDS	Lithium dodecyl sulfate
MHC-II	Major histocompability complex II
MRP	Multidrug resistance protein
MVBs	Multivesicular bodies
d.nm	diameter in nanometer
NO	Nitric oxide
NPs	Nano particles
NTA	Nanoparticle tracking analysis
NuPAGE	Native-polyacrylamide gel electrophoresis
PBCA	poly(n-butylcyanoacrylate)
PBS	Phosphate buffer saline
PD	Parkinson's disease
PDI	Poly-dispersive index
Pen-Strep	Penicillin Streptomycin
PFA	Paraformaldehyd
P-gp	P-glycoprotein
PTX	Paclitaxel
RIPA	Radio-immunoprecipitation assay
RMT	Receptor-mediated transcytosis
RNA	Ribonucleic acid
ROS	Reactive oxygen species
SDS	Sodium dodecyl sulfate
SEC	Size exclusion chromatography
SPR	Surface plasmon resonance
TBS	Tris buffered saline

TEER	Trans-endothelial electrical resistance
Tf	Transferrin
TJ	Tight junction
Tsg	Tumor susceptibility gene
WR	Working reagent
WGA	Wheat germ agglutinin

1 Introduction

1.1 Epilepsy

Epilepsy is a neurological disease that affects more than 22 million people in the world (Q. Li et al., 2019). Epilepsy is characterized by unprovoked and recurrent seizures, resulting from a temporary dysfunction of the brain caused by abnormal synchronous neuronal activity that can be induced by several reasons (Doboszewska et al., 2019). Alterations in the structure and/or function in an epileptic brain makes it sensitive to developing spontaneous seizures (Jefferys, 2010). In this section, it will be briefly discussed some of the reasons causing the development of epilepsy.

Blood-brain barrier (BBB) disruption, leading to increased permeability, increased vesicular transport, increased metabolic demand coinciding with reduced energy supplied to neurons is known to be associated with epilepsy (Hubbard & Binder, 2016). Additionally, the failure of Ca^{2+}-, K^{+}-, and N^{+}-pumps lead to neuronal depolarization (Hubbard & Binder, 2016). Alterations in K^{+} homeostasis and increase in the concentration of K^{+} in extracellular space, even in small amounts, enhance epileptiform activity. A rise in K^{+} and Ca^{2+} in the intercellular space results in dysfunction of glutamate receptors (Kovacs, Heinemann, & Steinhauser, 2012). Glutamate is an important excitatory neurotransmitter which is necessary for synapse formation and information processing. Abnormal concentrations of glutamate in the extracellular region of the brain is one of the reasons leading to epilepsy in humans, and during epileptic seizures, high glutamate concentration is observed (Soukupova et al., 2015). Studies also show that seizures are associated with boosted formation of reactive oxygen species (Dutta, Warshell, Bandypadhyay, Dutta, & Chandran) and nitric oxide (NO) (Kovacs et al., 2012). Gap junctions (GJs) are membrane channels consisting of connexin proteins that ensure direct exchange of metabolites and information between neurons and astrocytes. Previous studies show that regulations of blockers and openers of GJs have a significant impact on formation of epileptiform activity (Q. Li et al., 2019).

1.2 Structure and function of the BBB

Vessels in the central nervous system (CNS) are surrounded by the endothelial cells with unique properties that make them suitable to tightly regulate transport of molecules, ions and cells between the blood and the brain (Daneman & Prat, 2015). The BBB is a part of the microvasculature system of CNS in the brain that consists of three different cellular elements: BBB-endothelial cells, astrocytes, and pericytes (figure 1.1). These three cells form a capillary-like structure (CLS) (Ballabh, Braun, & Nedergaard, 2004). Optimal function of the BBB and formation of the CLS is dependent on the direct association of endothelial cells with astrocytes. Astrocytes are glial cells which interact with the endothelial cells on the brain side, and these cells are associated with maintenance of the BBB integrity (Ballabh et al., 2004). Pericytes are also attached to the endothelial cells and play a role in regulating cerebral blood flow (Ballabh et al., 2004). Endothelial cells are held by junctional complexes, including adherence junctions (AJs) and tight junctions (TJs) (figure 1.1) (Abbott, Patabendige, Dolman, Yusof, & Begley, 2010). Cadherin proteins in the AJs enable this part for the integrity of tissue structure and provide cell attachment. TJs is the other part of a junctional complex, consisting of proteins occludin and claudins located in the intracellular cleft and junctional adhesion molecules (JAMs). TJs make the endothelial cells responsible for the intense limitation of ions, polar solutes and macromolecules. Also, claudin proteins located in TJs contribute to the high electrical resistance throughout the endothelium (Abbott et al., 2010). The normal function of specific ion channels and transporters located within the BBB is critical for proper neuronal function (Hubbard & Binder, 2016)

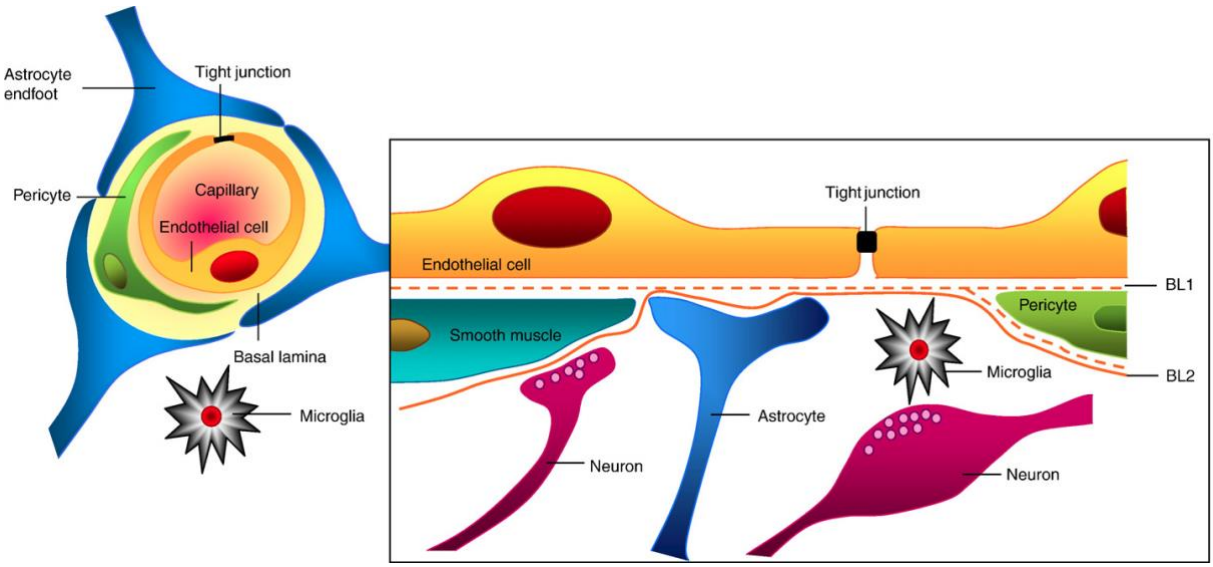

Figure 1.1. Cell composition of BBB. Capillaries that convey blood to CNS are surrounded by endothelial cells bounded together by TJs, pericytes that give the endothelial cells structural support and astrocytes that have a role in signaling to neurons. BL: basal lamina. Source: (Hubbard & Binder, 2016), adopted on 21.03.19.

The endothelial cells in the BBB have unique properties such as lack of fenestration and having more extensive TJs that making them different from endothelial cells in other tissues. (Ballabh et al., 2004). Some factors affect the ability of molecules to penetrate the CNS. Diffusion of lipid-soluble molecules through the BBB is easier than compounds with a high polar surface area. The cationic nature of bases and the interaction of them with negatively charged head groups of phospholipids give them more affinity than acids to pass the BBB (Abbott et al., 2010). O_2 and CO_2 gases diffuse across the BBB in the opposite direction of their gradients. Solutes with large molecular weight like peptides and proteins can cross the BBB via transcytotic mechanisms. These mechanisms can be either receptor-mediated transcytosis (RMT) or adsorptive-mediated transcytosis (AMT). During RMT, macromolecular ligands bind to specific receptors and trigger together into the endothelial cells. Endocytosis via AMT requires an extra positive charge on the macromolecule that induces interaction of molecule to the binding site on the surface (Abbott et al., 2010).

1.3 Mechanism of drug resistant epilepsy

Antiepileptic drugs (AEDs) suppress seizures by repressing abnormal excitation in the brain (Boets, Janssens, Lavreysen, & Steckler, 2105). Some of the traditional drugs used for the treatment of epilepsy are levetiracetam, carbamazepine, lamotrigine, topiramate, valproic acid, and fosphenytoin. The targets of most current AEDs are neuronal Na^+ and Ca^{2+} channels, glutamate receptors or γ-aminobutyric acid complex (Q. Li et al., 2019). However, there are some difficulties related to treatment with current AEDs, and more than one-third of epilepsy patients show resistant to the available treatments (Q. Li et al., 2019).

As several conditions are involved in the development of epilepsy, it's pathogenesis is also multifactorial, and several variables should be mentioned during treatments (Kwan & Brodie, 2005). Thus, there is no single reason for why some people respond to a drug, while there are patients which tried multiple drug trials without any remarkable reduction in seizure frequency

(Loscher, 2005). However, there are numerous hypotheses explaining the drug resistance in epilepsy. Drug-transporter hypothesis and drug-target hypothesis are the two major hypotheses related to this issue (Loscher, 2005). The drug-transporter hypothesis suggests that overexpression of efflux transporters prevent AEDs from reaching their targets in the CNS. P-glycoprotein (P-gp) and multidrug resistance proteins (MRPs) are both members of the adenosine triphosphate (ATP)-binding cassette (ABC) protein superfamily. Overexpression of P-gp and several members of MRPs in BBB endothelial cells seems to have significant roles on the efflux of their substrates back to the extracellular space (Kwan & Brodie, 2005; Loscher, 2005). The substrates of P-gp proteins are hundreds of compounds, such as drugs, nutrients, amino acids, sugars, peptides, pigments, metals, etc. (Kwan & Brodie, 2005). Meanwhile, the drug-target hypothesis assumes that alterations in drug targets in some patients may lead to loss of their sensitivity and thereby provide resistance to the AEDs. To explain this hypothesis, the effect of carbamazepine (CBZ) on Na^+ channels of neurons is considered as an example (Loscher, 2005). Substantial upregulation of Na^+ currents caused by abnormal function of Na^+ channels is associated with the process of epileptogenesis or in the maintenance of the epileptic state (Mantegazza, Curia, Biagini, Ragsdale, & Avoli, 2010). AEDs such as CBZ block the Na^+ channels and thereby inactivate the fast Na^+ currents. However, the Na^+ channels seem to be insensitive or less sensitive to the drug in patients with CBZ-resistant (Loscher, 2005).

1.4 Challenges of the existing delivery systems for the transport of therapeutics across the BBB

During last decades, researchers have acknowledged the potential of drug delivery approaches allowing delivery of therapeutics across the BBB (Teleanu, Chircov, Grumezescu, & Teleanu, 2019). Some strategies have been developed to overcome the challenges related to the delivery of pharmaceutical products across the BBB and reaching their targets in the CNS (Bhatt & Narvekar, 2018). One of these strategies is the mechanical disruption of the BBB that include, for example, usage of microchip systems and temporary disturbance of the BBB. There are many disadvantages associated with this strategy: dangers of contamination, CNS infection, toxicity and harm to cerebrum tissue are some of them (Bhatt & Narvekar, 2018). Another approach for transporting drug through the BBB is a modification of drug to form its active prodrug, which is suitable for penetration into the BBB. An example of drug modification is

the improvement of the lipophilic nature of the drug. The main disadvantage of this method is that increased lipophilicity of drug molecule enhances its metabolism, and thus, cause active clearance by efflux proteins located in BBB (Bhatt & Narvekar, 2018). The other physiological strategy is the utilization of carriers such as antibodies, lectins, sugars, and transferrin (Tf) proteins. These ligands can target specific receptors on the surface of endothelial cells of the barrier, and thus, they can provide delivery of drug molecule across BBB (Bhatt & Narvekar, 2018).

Despite the wide variety of strategies developed for the delivery of drugs across the BBB, the most effective characterized approach are nanocarrier drug delivery systems (Bhatt & Narvekar, 2018). Liposomes, nano-micells, exosomes, and nanoparticles are commonly used nanocarrier drug delivery systems explored in drug transport to the CNS (Bhatt & Narvekar, 2018; Niu, Chen, & Gao, 2018). Liposomes are small vesicles made of one or more phospholipid bilayers where the aqueous core is enclosed by a hydrophobic membrane (Tam, Sosa, Liu, Yao, & Priestley, 2016). Liposomes are noteworthy transport systems due to their simplicity of preparation, high bioavailability, and low toxicity. Also, both hydrophilic and lipophilic drugs can be loaded on liposomes. Thereafter, this nanocarriers represent a promising approach for the delivery of DNA and drugs to the brain (Alyautdin, Khalin, Nafeeza, Haron, & Kuznetsov, 2014). Additional modifications of liposomes involving treatment with an antibody or specific ligands may help them to be recognized by the BBB receptors, and facilitate the CNS delivery of drugs that are P-gp substrates (Alyautdin et al., 2014; Tam et al., 2016). For example, the (Tf)-modified liposomes significantly promoted the penetration of α-Mangostin in Alzheimer's disease (AD) studies (Niu et al., 2018). Liposomes have also been used to deliver Doxorubicin (Dox), a drug for a primary and metastatic brain tumor (Alyautdin et al., 2014). However, there are limitations including fast systemic elimination, possible instability and less control over the drug release, that restrict their utilization in some cases (Tam et al., 2016).

Organic and nonorganic nanoparticles are the other synthetic systems in treating neurodegenerative diseases (Niu et al., 2018). Nanoparticles of different types are useful vehicles in drug delivery as they are small in size, deliver the drugs in their active form to the specific site and have relatively high drug loading affinity (Niu et al., 2018). Loading of poly(n-butylcyanoacrylate) (PBCA) nanoparticles with rivastigmine, a drug to treat AD, showed higher brain delivery of the drug compared to the free drug (Alyautdin et al., 2014). The

drawbacks of using nanoparticles as delivery systems are their high toxicity, and that the distribution and degradation of nanoparticles in the brain are risk factors (Niu et al., 2018). The discovery of exosomes as natural nanocarriers in the drug delivery field will be discussed in the next sections.

1.5 Exosomes

As mentioned in section 1.2, the CNS is highly protected from penetration of many unwanted components, including drugs. The internalization is restricted by the presence of very specific transporters located on the BBB. On the other hand, these receptors are target for drugs developed for the treatment of neurological disorders is the CNS. Some of the approaches for drug-delivery to the CNS is discussed in the previous section. In this section, biogenesis and functions of exosomes as a delivery system will be discused.

1.5.1 Biogenesis of exosomes

Cells release three types of extracellular vesicles (EVs) according to a specific stimulus or as a part of normal cellular processes (Farooqi et al., 2018). Apoptotic bodies (ABs) with a diameter range from 1000-5000 nm are EVs that are secreted from the plasma membrane as a result of apoptosis. Microvesicles (MVs) are the other type of EVs with a diameter of 50-1000 nm. MVs are separated from plasma membrane often from injured or transformed cells. The third type of EVs are exosomes originating from inward budding of multivesicular bodies (MVBs) made directly by the plasma membrane (figure1.2, a) (Aryani & Denecke, 2016). MVBs or endosomes arise from the plasma membrane (Barile & Vassalli, 2017), which may undergo different processes in the cell. They can either merge with lysosomes where their contents degrade, or with the plasma membrane which yields exosomes from the cell to the extracellular side of the membrane (figure 1.2, a) (Farooqi et al., 2018). Exosomes with a diameter of 50-100 nm are known to be the smallest EVs (Aryani & Denecke, 2016; Barile & Vassalli, 2017). However, the size range for exosomes is also reported 30-150 nm (Farooqi et al., 2018) or 40-100 nm (Ha et al., 2016).

Exosomes can be identified or detected by their exosomal proteins which are not found or found at low levels elsewhere (Edgar, 2016). These proteins include the tetraspanin proteins (cluster of differentiation 9 (CD9), CD63, CD81, and CD82) that are essential for the transport of exosomes and binding of them to the target cells. Heat shock proteins (HSP70 and HSP90) are other proteins located on the exosome membrane which are involved in the biogenesis of MVBs (Figure 1.2, b). GTPases are associated with membrane fusion and transportation (Aryani & Denecke, 2016; Barile & Vassalli, 2017). Major histocompatibility complex II (MHC-II) is associated with T-cell specific responses (Farooqi et al., 2018). The other components of exosomes are cytoskeletal proteins (i.e., actin, tubulin, cofilin and profilin), enzymes (i.e., glyceraldehyde-3-phosphate dehydrogenase (GAPDH) and pyruvate kinase), integrins, annexins, flotillin and different RNA molecules (Figure 1.2, b) (Farooqi et al., 2018). Between these proteins, HSP70, CD9 and CD63 are commonly used reference markers of exosomes (Tamkovich, Tutanov, & Laktionov, 2016).

As the exosomes contain unique proteins, also the lipid composition of exosomes differs from that of the plasma membrane of the parental cell (Farooqi et al., 2018). Phosphatidylcholines, sphingomyelins, lysobis-phosphatidic acid, phosphatidic acid, cholesterol, ceramide, and phosphoglycerates are the lipids found on the exosome membranes (Farooqi et al., 2018). Exosomes reach their target cells by traveling through body fluids such as blood, saliva, synovial fluid, amniotic fluid, and can serve as long-distance communication in the body (Farooqi et al., 2018). However, they are also found in other body fluids like breast milk, urine, sperm, and follicular fluid and are secreted by a wide variety of cell types (Farooqi et al., 2018).

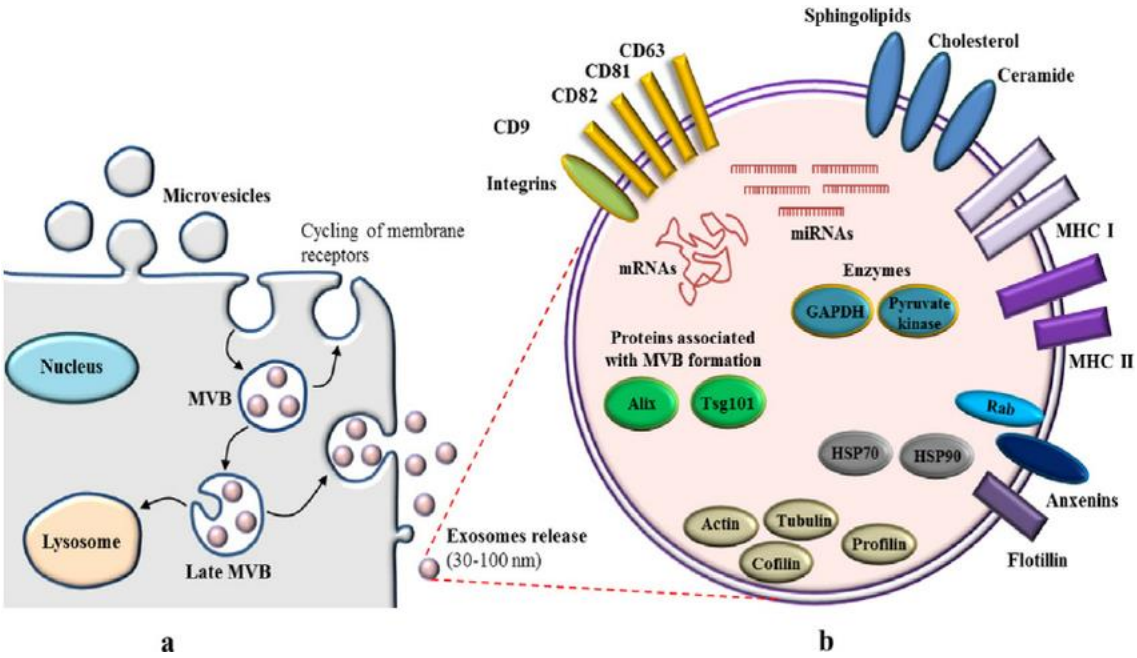

Figure 1.2. Origin of exosomes form membrane (a) and biomarker proteins on the surface of exosomes (b). Exosomes originate from inward budding of MVBs and are secreted into extracellular spaces. The illustration shows lipid composition of exosomes (sphingolipids, cholesterol and carbamide) and protein composition of exosomes (tetraspanin proteins; CD9, CD82, CD82 and CD63, heat shock protein; HSP70 and HSP90 and other proteins associated with exosome membrane; MHC I, MHC II, integrins, flotillin and annexins and enzymes; GAPDH, pyruvate kinase, tubulin, actin, profillin and cofilin. Abbreviations: MVB; multivesicular body, CD; cluster of differentiation, MHC; major histocompatibility complexes, GAPDA; glyceraldehyde-3-phosphate dehydrogenase, HSP70; heat shock protein 70, Tsg; tumor susceptibility gene. Source: (Giau & A.An, 2016), adopted on 19.01.19.

Uptake of exosomes by the receptor cells is a receptor-mediated process (Farooqi et al., 2018). When the receptor cell recognizes exosomes by the specific proteins located on their membrane, the exosomal lipids, such as phosphatidylcholine, interact with the complementary molecules found on the plasma membrane of cells. Then, the exosomes can release their content into the cytoplasmic space of the cell (Farooqi et al., 2018). Exosomes interact with their recipient cells via different mechanisms (Aryani & Denecke, 2016). The cargo of exosome can be delivered to the target cell via direct ligand-receptor interaction and without fusion into the membrane. In another mode of cargo delivery, the membrane of exosomes fuse into the membrane of the target cell resulting in the transportation of anchored proteins through the plasma membrane of the recipient cell. The other mode is endocytosis and transcytosis of exosomes in which vesicle contents are displaced in the target cell (Aryani & Denecke, 2016).

1.5.2 Exosomes as a nanocarrier

EVs, including exosomes, are natural delivery-systems for long-distance transport of nucleic acids, such as mRNA, miRNA and small RNA, proteins, antibodies and many other cargos in normal biological processes Ha, Yang, and Nadithe (2016). During the recent decades, the interest in using exosomes as a natural system for transfer of low molecular-weight drugs, nucleic acids, proteins, and other small molecules increased impressively (Barile & Vassalli, 2017). The benefits of using exosomes as nanocarriers for drug delivery are their specificity, small size, low toxicity, and that they can penetrate BBB. Exosomes have the trait to reach their targets, and they are able to deliver their cargo to the specific receiver cells (Luan et al., 2017). In addition, exosomes are also naturally stable (Ha et al., 2016) and can penetrate deep in tissues and evade the immune system (Farooqi et al., 2018). One of the most exciting properties of exosomes is their ability to cross the BBB as they can enhance the effectiveness of the drugs that need to pass the BBB for treatment of various neurogenerative disorders (Niu et al., 2018).

In a previous research, the therapeutic effect of catalase-loaded exosomes for the treatment of Parkinson's disease (PD) was studied (Haney et al., 2015). In this study, the exosomes originating from monocytes and macrophages and loaded by a potential antioxidant, catalase, showed significant neuroprotective effects in both *in vitro* and *in vivo* models of PD. In another investigation, exosomes derived from brain endothelial cell line (bEND.3) loaded with Dox and Paclitaxel (PTX) was tested for treatment of brain cancer in a zebrafish model (Yang et al., 2015). This study demonstrated that the fluorescent intensity of cancer cells and the tumor growth markers significantly decreased after treatment with exosome-delivered Dox and PTX.

However, the research on using exosomes as a natural nano-carrier is still at an early stage, and therefore many considerations should be taken before they enter into clinical practice (Niu et al., 2018). Exosomes originating from different cell sources have various lipid and surface protein composition (Luan et al., 2017). Hence, carefully studying of biological characteristics of exosomes emanated from different cell types is crucial. Otherwise, the predestinated effect of exosomal therapy or even the recipient cells or organ may be in danger (Luan et al., 2017). Production of exosomes in large-scale and *in vivo* studies regarding the potency and toxicology of exosomes still require further testing (Luan et al., 2017). Despite all these drawbacks, employing exosomes as nanocarriers is attractive and promising (Luan et al., 2017), and compared with other nanocarriers such as liposomes, they are more ideal due to their more

stability, overall biocompatibility and reduced toxicity (Farooqi et al., 2018; Ha et al., 2016). Additionally, more straightforward modification of exosomes because of the diversity of endogenous marker molecules and specific vector ligands make them more useful than liposomes to get over unfortunate targeting problem (Niu et al., 2018).

1.6 Basic principles of the used methods

The validation of a study is highly dependent on the methods applied. There is no single ideal technique for purification and characterization of exosomes, and a combination of several methods is recommended (Ha et al., 2016). In this investigation, size exclusion chromatography (SEC) was used for isolation of exosomes from plasma. For identification of exosomes, dynamic light scattering (DLS), gel electrophoresis and western blotting were used. Confocal laser scanning microscopy was utilized to visualize the isolated exosomes and to assess the internalization of them into the human cerebral microvascular endothelial cells (hCMEC/D3) cells. The basics of SEC, western blotting, DLS and confocal microscopy will be discussed in the following sections.

1.6.1 Basics of confocal microscopy

Confocal laser scanning microscopy is a powerful method that can be utilized for identification of cells and sub-microscopic cellular components (Price & Jerome, 2011b). A fluorochrome is a molecule that absorbs a photon with a particular wavelength and emits a photon with less energy than the absorbed photon. The emitted photon can be observed as fluorescence (Price & Jerome, 2011b). For a single molecule, absorption occurs only if the inflicted light is able to excite the fluorochrome from ground state to a higher energy state. The atomic organization of the molecule restricts wavelengths that can produce an excited state in an individual molecule (Price & Jerome, 2011b). This phenomenon makes it possible to identify the fluorescent molecules based on their excitation and emission energies. Use of specific wavelengths of light and pinholes to eliminate out of focus light make it possible to gain images with high contrast and more details such as small structures and molecules (Price & Jerome, 2011f).

The setup of a confocal microscope is generally as following; laser, objectives, filters, detectors, and specimen (figure 1.3) (Price & Jerome, 2011b). Light path in the instrument begins from a laser source. Laser light, that represents the stimulated emission, and produced by the source is the excitation source. The light coming from the laser passes through a pinhole aperture. Then, it goes through an excitation filter that is situated for separating the different wavelengths of light, and unnecessary wavelength/s is/are restricted (Price & Jerome, 2011b). A dichromatic mirror is the next part, which is situated to reflect the light back to the focal plane of an objective lens that focuses the excitation light onto the specimen. The light emitted by the fluorochrome travel back to the dichromatic mirror. The emission lights have a longer wavelength and less energy than the excited light and thereby, they are transmitted through the mirror. Next, they reach to the filter placed on the other side of the dichromatic mirror which limits the wavelengths, and then they are focused as a confocal point at the detector pinhole aperture before signals finally reach to the detector (see figure 1.3) (Price & Jerome, 2011b)

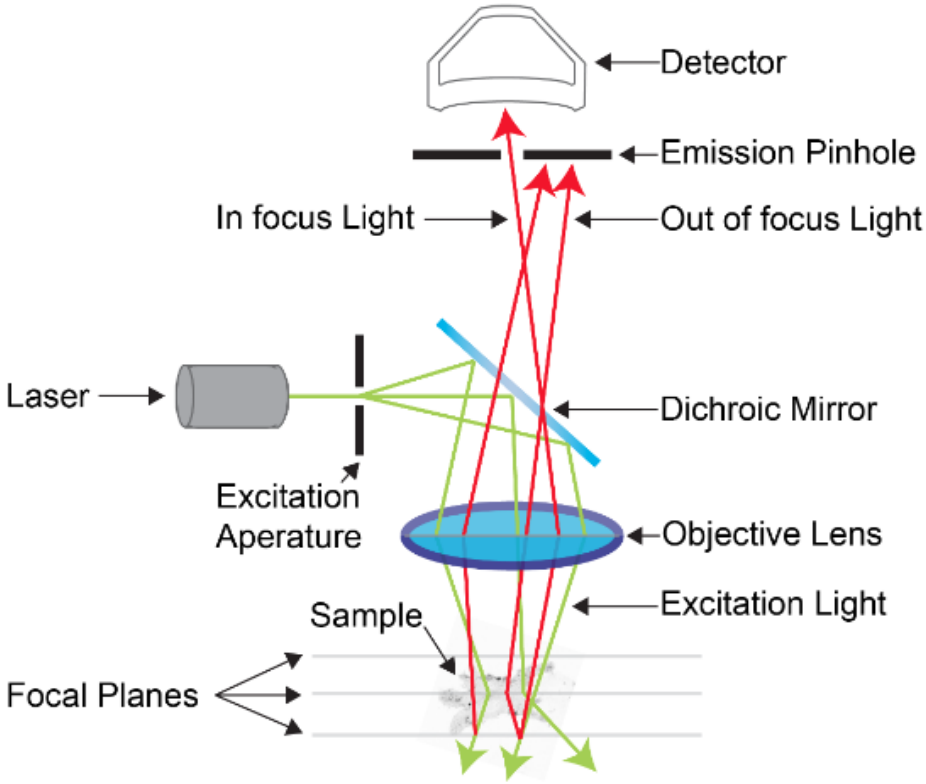

Figure 1.3. A simple diagram showing the general setup of a laser scanning confocal microscope. The laser coming from the source path through a pinhole and an excitation filter before it catches to a dichromatic mirror and then an objective before it reaches the sample. Then, the emitted light from sample path back through the objective, emission filter and finally, is focused on the detector by the detector pinhole. Source: https://imb.uq.edu.au/facilities/microscopy/hardware-software/confocal-microscopes, adopted at 15.05.19.

Many factors affect the reliability and quality of the images taken by the confocal microscope (Price & Jerome, 2011e). Using suitable techniques for preparation of specimen is one of the important factors that depend on the application of confocal imaging (Price & Jerome, 2011e). Actually, it is not easy to define a single best method for sample preparation. It depends on for example; the labeling techniques, cell or tissue type and type of data that will be obtained. During the preparation of fixed samples, the choice of suitable fixative is important. Two types of fixatives are available; precipitating fixatives such as organic solvents and those that cross-link proteins like aldehydes. Both can be useful for the confocal experiment, but formaldehyde and glutaraldehyde solutions are the most common fixatives for confocal imaging. This type of fixation involves the creation of networks that link the cellular constituents and maintain structural integrity. Fixation with (3-10%) formaldehyde is most common for confocal microscopy (Price & Jerome, 2011e). The other factor affecting the quality of an image is the proper setup of the operating parameters on an instrument (Price & Jerome, 2011d). Table 1.1 gives an overview of the operating parameters which affect the quality of the image taken by the confocal microscope. Operating parameters should be adjusted such that the digital images taken represent the scanned images through the microscope (Price & Jerome, 2011d). Additionally, laser unit, objective characteristics, dye interactions, pinhole diameter, detectors etc. are other factors that may affect the quality of confocal images (Price & Jerome, 2011c).

Table1.1. Adjustments of the operating parameters, advantages and disadvantages of them during confocal imaging. The table is adapted from (Price & Jerome, 2011d).

Parameter	Advantage	Disadvantage
Decreased laser output	Improved S/N ratio	Increased specimen damage
Increased scan speed	Improved S/N ratio	Increased scan time and specimen damage
Line or frame averaging	Improved S/N ratio	Increased scan time and specimen damage
Increased pinhole size	Improved S/N ratio	Decreased contrast and resolution in x, y and z
Increased number of pixels (smaller pixel size)	Improved resolution	Increased scan time, large file size
Increased amplifier gain	Fewer photons required	Poor S/N ratio
Increased amplifier offset	Improved gamma	Decreased contrast
Narrow band pass filter	Minimal bleedthrough	Decreased signal
Sequential imaging	Eliminates bleedthrough	Increased scan time and specimen damage

Simultaneous imaging	Decreased scan time and specimen damage	Increased bleedthrough of fluorochromes with overlapping emission spectra
Long wavelength fluorochrome	Improved depth of imaging	Decreased resolution
Short wavelength fluorochrome	Improved resolution	Decreased depth of imaging

It is conceivable to produce three-dimensional representations of the subjects by scanning serial planes at different depths. In practice, single vertical slices (z-series) are obtained by scanning a combination of with (x), length (y) along with depth (z). In a single image, the z-dimension is infinitely thin, and there are empty spaces between a series of images. To fill these empty spaces, the 2D image is stretched along z-dimension (figure 1.4). How many details can we see in a 3D visualization, depends upon units of optical slices in the projection image. More optical slices supply more interior details than fewer optical slices in the final image (Price & Jerome, 2011a).

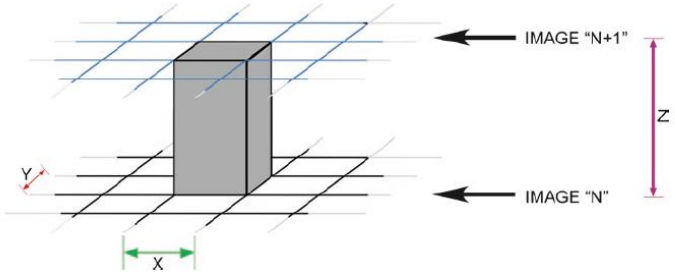

Figure 1.4. Illustration of x, y and z dimensions in 3D image by confocal microscope. Source: (Price & Jerome, 2011a), adapted at 03.05.19.

1.6.2 Gel electrophoresis and Western blotting

Electrophoresis is a widely used method for separating proteins, DNA and RNA based on their size, and that carries out in gels containing porous made by polyacrylamide (Berg, Tymoczko, & Stryer, 2012). In the first step of gel electrophoresis, proteins are denatured using sodium dodecyl sulfate (SDS), an anionic detergent, that break the 3-D structure of proteins and make SDS-protein complex with a net negative charge. Then, the SDS-protein complex is subjected in the electrophoresis and an electric field is applied to the gel. The mobility of polypeptide chains is based on their size such that large proteins are nabbed by the pores on the gel and stay on the top while the small proteins move rapidly through the gel. Finally, the proteins can be

visualized by staining them with dyes such as Coomassie blue, or they can be transferred to a membrane for immunoblotting (Berg et al., 2012).

Western blot, an immunoassay technique, is traditionally used for detection of a protein using an antibody that is specific for the protein (Kurien & Scofield, 2006). In the blotting, proteins separated by gel electrophoresis are electrophoretically transferred to a membrane such as nitrocellulose membrane. For this purpose, the gel is placed on the membrane and filter papers are placed on top (cathode) and bottom (anode) of them. Next, the proteins on the membrane can be probed with the antibody specific for the protein of interest. The antibody-protein complex can be detected by adding a secondary antibody conjugated with horseradish peroxide (HRP) to the sheet following by incubation in luminol containing enhanced chemiluminescence (ECL) solutions. A reaction between luminol and peroxide in HRP make chemiluminescent detection of the protein possible (figure 1.5) (Kurien & Scofield, 2006).

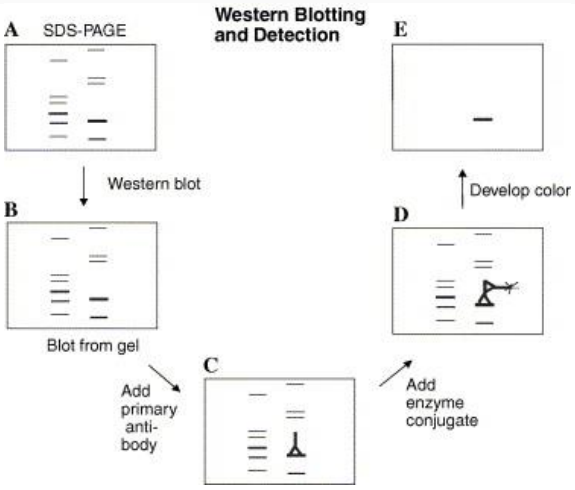

Figure 1.5. Illustration showing steps in western blotting. Size based separation of protein by gel electrophoresis (A). Transfer of protein to the membrane (B). Addition of primary antibody (C). Addition of enzyme (HRP)-conjugated secondary antibody (D). Detection of the protein of interest (E). Source: (Kurien & Scofield, 2006), adapted at 25.04.19.

1.6.3 DLS

Investigation on particle size determination is important during the development of nanoparticles as drug delivery systems (Bhattacharjee, 2016). DLS is a powerful technique to

measure the size of colloids, nanoparticles and molecules, and offer an easy and reproducible tool for characterization of nanoparticles based on their size (Bhattacharjee, 2016).

The detected light in DLS is the result of scattered light, by particles, that sourced from a laser and after performing some mathematical algorithms is given to an autocorrelator. When the particles within dispersion and with continuous mobility scatter light, constructive and destructive interferences are generated and provides a fluctuation of scattering intensity over time. Hence, the intensity autocorrelation function (ACF) often written as $G2(\tau)$ and is expressed as Eq. (1):

$$G2(\tau) = 1 + G1(\tau)^2 \quad (1)$$

Here, τ = time intervals and G1 = field correlation function.
In the correlogram generated in DLS instruments, the ACF [$G2(\tau)$] is calculated by data obtained from the sample and then the translational diffusion coefficient (D_t) can be calculated using Eq. (2):

$$G2(\tau) = 1 + b.e^{-2D_t q^2 \tau} \quad (2)$$

Where, q = scattering vector, b = constant dependent on the instrument and settings of optics.
Finally, the hydrodynamic radius (R_H) of particles can be obtained from Eq. (3):

$$D_\tau = \frac{k_B T}{6\pi\eta R_H} \quad (3)$$

Where, k_B = Boltzmann constant ($1.38064852 \times 10^{-23}$ J/K), T = temperature and η = absolute viscosity. The DLS results for a particular sample are dependent on factors such as temperature, viscosity of the solvent, type of instrument, inter-particular interactions depending on solvent, and concentration of nanoparticles (Bhattacharjee, 2016).

Different scattering instruments are developed for different purposes, but all of them have three major components; laser, sample and light detector (Bhattacharjee, 2016). The laser used is a He-Ne laser with a wavelength of 633 nm and a laser source providing a stable beam of monochromatic light. The power of the laser can be altered by an available attenuator. A transparent, homogenous and clean sample with a sufficient volume is required in order to

obtain data with good quality (Bhattacharjee, 2016). The minimal volume required, and type of cuvettes varies with the model (Bhattacharjee, 2016). Cuvettes made of plastic with inbuilt electrodes, scratch-free glass and optically translucent plastic are available for use (Bhattacharjee, 2016). The instruments are equipped with detectors placed at 173° angles that detect backscattering and thereby are able to exclude excess scattered light. There is also a focusing lens available that select the illuminated area of the sample to alter the path length of the scattered light before it reached to the detector (figure 1.6) (Bhattacharjee, 2016).

The advantages of the DLS technique are; requirement of minimal sample preparation, pre-experimental calibration is not essential, and the technique is non-invasive, user-friendly digital interference (Bhattacharjee, 2016). The limitation of DLS is its low resolution especially for samples containing polydisperse particles (Bhattacharjee, 2016). To get a peak by DLS, different in particle size should be at least a factor of 3 (e.g., 50 and 150). To get a better resolution, particles can be size-separated prior to DLS analysis (Bhattacharjee, 2016)

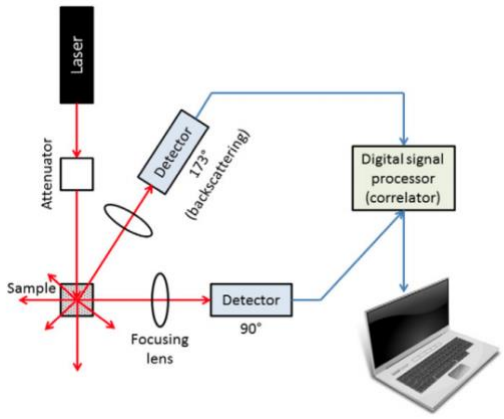

Figure 1.6. Illustration showing the general setup of an DLS instrument. Laser, attenuator, sample, detector, correlator and a computer with operating software are the main components of an DLS instrument. Source: (Bhattacharjee, 2016),adapted at 30.40.19.

The homogeneity of the particles in a sample can be determined by the data obtained from DLS and is denoted as the poly-dispersity index (PDI). Also, PDI- value gives information about width of the particle size distribution. The PDI-values of 0.1- 0.4 are mid-range numbers, and refer to moderately polydisperse, while values > 0.4 are considered to be highly poly-disperse and with low quality (Bhattacharjee, 2016).

1.6.4 Isolation of exosomes

Several techniques are developed for isolation of exosomes in different studies. Exosomes are isolated with different techniques for several purposes such as studying their density, shape, size and characterization of their surface proteins (P. Li, Kaslan, Lee, Yao, & Gao, 2017).

Ultracentrifugation is a common technique used for exosome isolation. When a centrifugal force is applied, particles in the suspension will be separated based on their density, size and shape. Human plasma or serum is cleaned prior to the start of isolation to remove large bioparticles in the sample. Then with applying a centrifugal force, particles including exosomes move as individual zones, according to their specific sedimentation rate. Finally, the isolated exosomes can be separated by a simple fraction collection (P. Li et al., 2017). The most disadvantages of this technique are possible contamination with other EVs and exosome loss during removal of supernatants (P. Li et al., 2017).

The other popular technique, which is faster than ultracentrifugation, is the isolation of exosomes dependent on their size or molecular weight using membrane filters with defined molecular weight or size exclusion limits. This popular technique is called ultrafiltration. In ultrafiltration, exosomes can be isolated using membrane filters with defined molecular weight or size exclusion ranges (P. Li et al., 2017). The main drawback of ultrafiltration is deformation and breaking up of large vesicles (P. Li et al., 2017).

Another size-based isolation technique which offers isolation of relatively uncontaminated EVs from plasma is SEC (P. Li et al., 2017; Stranska et al., 2018). In SEC exosomes are separated on the basis of size using e.g., qEV-original columns (Boing et al., 2014). In this type of column, a mobile phase that is the sample in phosphate buffer saline (PBS) buffer goes through a stationary porous phase to be separated based on their size. The column is suitable for separation of components in serum, plasma, saliva, urine, and cell culture media. Smaller molecules are nabbed by pores and elute later than larger molecules such as exosomes that are not able to pass through pores and elute from the column first. The first 3.0 ml buffer going through the column is void volume. Collecting of fractions containing exosomes starts after 3.0 ml, such that 0.5 ml is collected in each fraction. It is expected that the next 3.5 ml after void volume contains exosomes (Boing et al., 2014). The benefit of SEC compared to differential centrifugation is less risk of protein complex formation and vesicle aggregation. Also, SEC

confers exosome samples with good recovery (43% ± 23) and unaffected biological properties after isolation (Boing et al., 2014). The main limitations of SEC are the low vesicle yield and probable contamination with lipoproteins in the isolated fractions (Stranska et al., 2018)

1.6.5 Cell culture

Cell culture, in general, require specific techniques and equipment in the laboratory, and the precise category required depends on the cell line and proposes of the work. Microbiological safety cabinet, centrifuges, incubators, disinfectants, sterile tubes and pipettes are used routinely as the most important pieces for cell culture.

As mentioned in section 1.2 low permeability of BBB is the major challenge in the transport of the drug across BBB into the CNS. To assess the penetration of the nanocarriers drug delivery system into the BBB, *in vitro* BBB models are developed (Eigenmann et al., 2013). For this purpose, immortalized hCMEC/D3 are cultured in this investigation. The availability of primary culture from the human origin is a limited issue, and hence, using immortalized human brain capillary endothelial cells is the other alternative for studying the permeability of BBB as the early steps of drug development (Eigenmann et al., 2013). hCMEC/D3 showed promising results in previous researches according to study the penetration of drugs into the brain (Eigenmann et al., 2013) as they provide stable, easily grown and transferable cell lines that maintains a normal BBB phenotype (Weksler, Romero, & Couraud, 2013). Expression and activity of the BBB-transporters such as ABC-transporters, p-gp and MDRs are indicated in hCMEC/D3 cell lines (Poller et al., 2008). However, results achieved from culturing cells *in vitro* can be less reliable compared to results obtained from *in vivo* conditions that is the limitation of cell-line based BBB models (Weksler et al., 2013). For example, hCMEC/D3 cells showed low trans-endothelial electrical resistance (TEER) values compared to *in vivo* conditions (Weksler et al., 2013).

1.7 Aims of the study

The two main aims of this thesis were:

1. To isolate and characterize the isolated vesicles, expected to be exosomes and
2. To investigate the BBB permeability of the isolated vesicles using hCMEC/D3 as a model.

2 Experimental

2.1 Materials

2.1 Exosome isolation

Name	Content	Description/producer
10x PBS pH 7.4	NaCl 80 g/L KCl 2.0 g/L Na_2HPO_4 14.4 g/L KH_2PO_4 2.0 g/L	10x PBS stock solution was autoclaved and degassed before use. For all experiments 1x PBS were used.
20% Ethanol	19% ethanol (95%) 80% dH_2O	2 mL on top of the column during storage
qEV size exclusion column		Purchased from iZON Science
Plasma		From an epileptic human donor

2.2 Gel electrophoresis and western blotting

Homemade		
Name	**Content**	**Description**
10x TBS buffer	1M Tris-HCl pH 7.5 5M NaCl dH_2O	For all experiments 1x TBS was used, and it was made by diluting 10% 10x TBS into 90 % dH_2O.
1x Transfer buffer	96 mM Glycine 10 mM Tris	For transferring proteins from gel to the membrane, 20% methanol was added to 80% 1x transfer buffer.
CBB staining	0.02 % (w/v) CBB g-250 5%(w/v) Aluminiumsulfat (14-18) hydrate 10% (v/v) ethanol (96%) 2% (v/v) Orthophosphoric acid (85%)	Staining the gel
5% TBS milk	5% Dry milk 95% 1X TBS	Blocking of membrane
ECL1	2M Tris pH 8.3 Couric acid Luminol	Keep Luminol in the dark, and use fume hood for making the solution

	dH_2O	
ECL2	2M Tris pH 8.3 H_2O_2 dH_2O	
1x RIPA lysis buffer	20 mM Tris-HCL (pH 7.5) 150 mM NaCl 1 mM Na_2EDTA 1mM EGTA 1% NP-40 1% sodium deoxycholate 2.5 mM sodium pyrophosphate 1 mM β-glycerophosphate 1 mM Na_3VO_4 1 μg/ml leupeptin	
Ready purchased		
Name	**Description/ Producer**	**Lot. no**
Blot 10% Bis-Tris NuPAGE MES gel	Invitrogen™	18092071
10x SDS loading buffer	NOVEX	1920967
4x LDS sample buffer	NOVEX	1945839
20x MES SDS running buffer	NOVEX	1936408
HSP70- antibody	Dilution factor: 1: 1000, SBI	Cat. no. EXOAB-Hsp70A-1
Goat Anti-Rabbit HRP secondary antibody	Dilution factor: 1:7500, SBI	Cat. no. EXOAB-TSG101-1
SeeBlue® Plus2 Prestained standard	Invitrogen	2020092

2.3 Cell culture

Name	Producer	Description/Lot. no
hCMEC/D3 cells	Millipore	LOT: RD1412004
1% Pen-Strep		
EndoGRO™Complete Media Kit	Millipore	Endo-GRO Basal medium can be stored on 2-8° C, and the rest of Components are stored in -20° C until use, Cat. no: SCME004-S.
Collagen, 3 mg/ml	Life Technologies	2029885
1XPBS		For coating of flasks and washing the surface of cells.
Trypsin		For trypsinization of cells.
Fibroblast Growth Factor (FGF) 2, 1ng/mL	Millipore	Supplemented with Endo-GRO™ Complete Media Kit, Cat. no. GF003
10 % DMSO		Added to media for freezing endothelial cells

Trypsin-EDTA 1x in PBS	Biowest	w/o Calcium, w/o Magnesium, w/o Phenol Red, Sterile Filtrated. Storage at -20° C. S18536L0940

2.4 Staining of exosomes and cells

Name	Producer	Cat. no
Wheat Germ Agglutinin (WGA) 488, 1mg/mL	Biotium	29022-1
Wheat Germ Agglutinin (WGA) 640, 1mg/mL	Biotium	29026-1
Hank's balanced salt solution (HBSS)	PAA	H15-009
antifade mounting medium with DAPI	Vectashield	LOT: ZF0219
Hoechst staining 33342, 2 mg/mL		
1x PBS and 1x PBS^{+} pH 7.4	homemade	
4% paraformaldehyde (PFA)	homemade	

2.5 Protein quantification

Name	Producer	Cat. no
BCA protein assay kit	Thermo Scientific	23225

2.2 Methods

2.2.1 Isolation of exosomes from blood plasma

Exosomes originating from human blood plasma was isolated by SEC using qEV-original columns. The column was prepared by placing it in a holder, leveling it and removing the 20% ethanol preserving the column. Then the bottom luer-clip and the top-cap were removed, and the column equilibrated with at least 10 mL of elution buffer (degassed 1x PBS). Cellular components of the plasma were eliminated by 2x centrifugation at 2500 xg, at 4° C, for 15 min. 500 µL cleared plasma was loaded on the column, and 0.5 mL of fractions were collected (figure 2.1). Fractions 1-6 represented the void volume containing apoptotic bodies and microvesicles, whereas fraction 7-13 were expected to contain exosomes and were characterized according to size and homogeneity by DLS and used for further analysis.

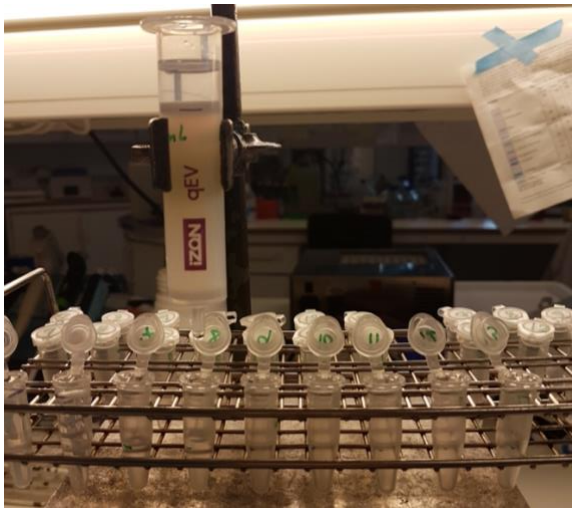

Figure 2.1. Isolation of exosomes by SEC using a qEV-original column. 0.5 mL of the sample resuspended in 1x PBS was collected in each fraction. Fractions 7-13 expected to contain exosomes and therefore were used for all analysis.

2.2.2 Dynamic light scattering

The DLS analyses were performed using a Zeta-Sizer Nano S instrument. 50 µL of exosome fractions resuspended in 1x PBS was added to a quartz cuvette, and the size distributions and homogeneity were measured at room temperature and at an angle of (137°).

2.2.3 Absorbance measurements

Isolated exosome fractions were diluted in a ratio of 1:20 and poured on wells of a Greiner UV star-SL plate. Absorbance was measured at 280 nm and 498 nm using a Spectra-Max Paradigm Multi-mode Microplate Reader (Molecular Devices).

2.2.4 Native PAGE gel electrophoresis and western blotting

Fractions assumed to contain exosomes based on the DLS analysis were prepared by addition of 4x LDS sample buffer, 10x reducing agent and heating at 70° C for 10 min. before loading on a Blot 10% Bis-Tris NuPAGE MES gel. The samples were separated at 200 V for 22 min. prior to characterization of total protein content by CBB staining and exosome specific proteins by western blotting techniques. To analyze the total protein content, the first gel was incubated with CBB staining solution for 1 h, rinsed 3x 5 min. in distilled water and then de-stained in de-staining solution prior to white light scanning by a LiCore instrument. Western blotting was performed by transferring the protein bands on the other gel to a nitrocellulose membrane using a fast blotter (Thermo Scientific), western-blotting apparatus. After transfer, the proteins were blocked on the membrane by incubating the membrane in 5%TBS milk for 45-60 min., and then the membrane was washed 3x 5 min. in 1x TBS. The membrane was incubated in HSP70 primary antibody diluted by a ratio of 1:1000 in 5%TBS milk at 4°C overnight. The following day, the membrane was washed 3x 5 min. in 1x TBS, prior to adding the secondary antibody Goat anti-Rabbit diluted 1:7500 in 1x TBS and incubating it for one hour at room temperature. Cheminulescent detection of HRP labeled HSP70 was performed using homemade ECL solutions (Table 2.2 in materials). Finally, the HSP70 immuno-reactive proteins were identified in a ChemiDoc^{TM} Toch Imaging System (Bio-rad).

2.2.5 Protein quantification

The concentration of the proteins was determined with a Bicinchoninic acid (BCA) kit. The Working Reagent (WR) was prepared by mixing 50 part of Reagent A and 1 part of Reagent B (ratio A: B = 50:1). A set of protein standard were made by diluting the bovine serum albumin

(BSA) standard and making different BSA concentrations (table 2.6). Then 200 μL of WR was added to 25 μL of exosomes resuspended in 1x PBS and diluted standards A-I in the wells of the microplate. The plate was covered and incubated at 37°C for 30 min. before cooling down to room temperature and recording absorbance at 562 nm in a Spectra-Max Paradigm Multi-Mode Microplate Reader (Molecular Devices).

Table. 2.6. Preparation of BSA standards

Vial	volume of diluent (μL)	Volume of source of BSA (μL)	Final BSA concentration (μg/mL)
A	0	300 of stock	2000
B	125	375 of stock	1500
C	325	325 of stock	1000
D	175	175 of vial B dilution	750
E	325	325 of vial C dilution	500
F	325	325 of vial E dilution	250
G	325	325 of vial F dilution	125
H	400	100 of vial G dilution	25
I	400	0	0 = blank

2.2.6 Concentrating and lysing of isolated samples

Amicon Ultra-0,5 mL centrifugal filter devices were used to remove the unwanted proteins and up-concentrate the isolated samples prior to preparing them for electrophoresis. 500 μL of sample was loaded on the filter and spent at 14,000 xg. The final concentration of the sample depends on the spin-time. Table 2.2.6.1 shows different spin times and concentrate recovery.

Table 2.7. Concentration factor (x) and the volume of concentrate are dependent on the spin time.

Spin time (min)	Concentration volume (μL)	Concentration factor (X)
5	58	9
10	19	26
15	15	33
20	13	36
30	11	41

To open the membrane of the isolated vesicles, radio-immunoprecipitation assay (RIPA) lysis buffer was used prior to gel electrophoresis. For this propose, the small volume (e.g., 8 μL if sample was 8 μL) of RIPA buffer was added to the samples following by sonication in 10 seconds. Then, the lysed samples were incubated at 4°C for 15 min. before they were prepared for electrophoresis.

2.2.7 Cell culture

2.2.7.1 Medium preparation

L-Glutamine and fetal bovine serum (FBS) were thawed in a water bath at 37°C. All flasks and vials were sprayed and wiped off before transferring them into the sterile bench. To prepare the Endo-GRO basal medium (Table 2.3) the components of the medium kit (L-Glutamine, hydrocortisone, hemisuccinate, heparin sulfate, ascorbic acid, FBS, endo-GRO-LS supplement and Rh epidermal growth factor (EGF)) were added. 1 ng/mL fibroblast growth factor (FGF) that was diluted in 1x PBS and sterile filtrated, was added to the medium separately.

2.2.7.2 Coating of flasks by Collagen

Collagen (10 ng/cm^2) was diluted in 1x PBS buffer, and a T75 flask was coated by 5 ml of collagen solution. The flask was incubated at 37°C in an 5% CO_2 humidified incubator for at least 1 hour before use.

2.2.7.3 Thawing of cells

The vial of hCMEC/D3 cells was removed from the liquid nitrogen tank and incubated in a 37°C water bath. When cells were completely thawed, the vial was disinfected with 70% ethanol prior to carefully transferring the cells to a sterile 15 mL conical tube using a 1 mL pipette. Then using a 10 mL pipette, 9 mL of hCMEC/D3 complete medium was added dropwise to the cells. The tube containing the cells was centrifuged at 300 xg for 3 min., and the supernatant was removed from the tube. The pellet containing cells was resuspended in 10 mL of pre-warmed hCMEC/D3 complete medium. Finally, the 1x PBS was removed from the

T75 flask prior to plating the resuspended cells in the medium into the flask and observed by a white light microscope (figure 2.2, a). The cells were incubated at 37°C in a 5% CO_2 humidified incubator.

2.2.7.4 Sub-culturing of cells

The medium was exchanged every two to three days after cultivation. Cells were observed by a microscope, and when they were about 80% confluent sub-culturing was performed (figure 2.2, b). To start with, the medium from T75 tissue culture flask was removed, and the surface of the confluent layer of hCMEC/D3 cells was washed with 6 mL 1x PBS. Then the cells were trypsinated by adding 3 mL of pre-warmed trypsin solution to the cells and incubating them for 3-5 min. in the 37°C in 5% CO_2 humidified incubator. After complete detachment of cells was observed in the microscope, 8 mL of pre-warmed hCMEC/D3 medium was added to the plate prior to transferring the cell suspension to a 15 mL conical tube. The tube was centrifuged at 300 xg for 5 min, resulting in the pelleting of the cells. The supernatant was removed, and cells were resuspended in 2 mL of hCMEC/D3 medium before cells were counted in a Muse® Cell Analyzer. Counted cells were either seeded in new coated flasks or were frozen in hCMEC/D3 medium containing 10% DMSO.

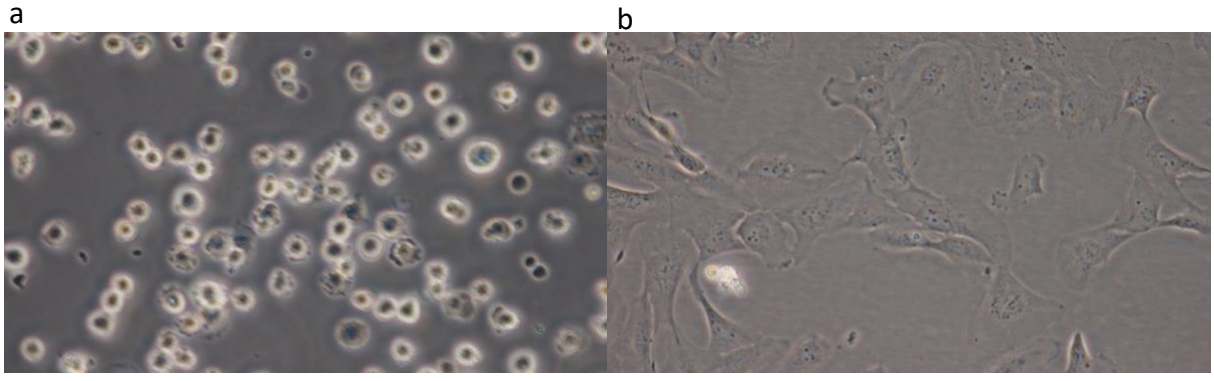

Figure 2.2. White light microscopy images of hCMEC/D3 cell line (Passage 3) in 40X objective immediately after cultivating (a) and 5 days after cultivating (b).

2.2.8 Staining of isolated exosomes

Staining of exosomes was performed with two different dyes, Hoechst and Wheat Germ Agglutinin (WGA) 488 separately and for different purposes but using the same protocol. 2-3 fractions of isolated exosomes (resuspended in 1x PBS) pooled and centrifuged at 16000 xg for 60 min at 4° C to achieve a pellet of exosomes. Then the pellet was washed twice with 1x PBS and twice with 1x PBS containing Ca^{2+} and Ma^{2+} (PBS^{+}). In each washing step, the pellet was resuspended in 200 µL of 1x PBS (or PBS^{+}) and centrifuged at 16000 xg for 30 min at 4°C. To stain the exosomes, a concentration of 5 µg/mL of stain was used and the exosomes in the staining solution were incubated in 37°C for 30 min. prior to washing them twice with 1x PBS^{+} at the same way as previous washings to remove the unbounded stains. A coverslip was coated with (10 ng/cm^2) collagen diluted in 1x PBS and incubated at 37°C for more than 2 hours. When the stained exosomes were ready, the 1x PBS was carefully removed from the coverslip, and the pellet resuspended in 100 µL of 1x PBS was placed on the coverslip and incubated for 30 min. at room temperature. 1x PBS containing exosomes was removed form coverslip, and the exosomes were fixed on coverslip by adding 4% paraformaldehyde (PFA) to it and incubating them for 15 min. at room temperature. The pipetting would be performed very gently and carefully due to preventing the loss of exosomes. In the end, 4% PFA was removed and the rest was air dried prior to mounting of the coverslip on a slide using 5µL Vectashield mounting medium.

2.2.9 Staining of hCMEC/D3 cells

The cells were cultivated on the sterile coverslips as in the section. 2.2.7.3, and when they were about 80% confluent, the medium was removed, and the cells were incubated in 20 µg/mL WGA 640 stain for 5 min. at room temperature. After incubation time was over, the cells were washed immediately and gently twice with Hank's balanced salt solution (HBSS). Then the cells were fixed on the coverslip by incubating them in 4%PFA for 15 min. at room temperature. Finally, the 4%PFA was removed from coverslip, and the rest was air dried prior to mounting the coverslip on a microscope slide with 5µL Vectashield mounting medium.

2.2.10 Confocal imaging

Visualization of vesicles stained with Hoechst and cellular uptake of the exosomes was performed using a A1R confocal laser microscope system with a water-immersion 60x objective and lasers 408 nm (DAPI), 488 nm (Alexa 488 water) and 640 nm (Alx647). Following wavelengths were used for the scanning of the samples:

DAPI → Excitation (Ex): 425 nm, Emission (Em): 475 nm

Alexa 488 water → Ex: 500 nm, Em: 550 nm

Alx647 → Ex: 663 nm, Em: 738 nm

Following settings were used for scanning and capturing the images:

→ HV; 120 ± 10

→ laser power; 2 ± 0,5

→ Offset; - 9 ± 2

3 Results

In this investigation, we performed characterization of exosomes isolated by SEC. The characterization was carried out using different techniques including DLS (for size distribution determination), western blotting (presence of exosome markers) and confocal microscopy imaging. To prove whether how long and in which condition, the exosomes preserved their size and homogeneity, we studied their alterations at different storage temperatures several days after isolation using DLS and absorbance measurements. Finally, exosome uptake by hCMEC/D3 cell line was assessed.

3.1 Characterization of exosomes

Identification of the isolated vesicles as exosomes is the first step in exosome research (Chia, Low, Wang, Li, & Gao, 2017). However, the reliability and accuracy of the identification and characterization of exosomes is a critical issue due to their small size. Thence, various techniques are developed to identify the exosomes based on their size, mass, density or on specific proteins presented on their surface (Chia et al., 2017). They are immunoaffinity capture (IAC), surface plasmon resonance (SPR), nanoparticle tracking analysis (NTA), DLS and other antibody-based methods (Chia et al., 2017). Meanwhile, DLS and immunoblotting were the utilized methods for characterization of the isolated vesicles as exosomes during this investigation.

3.1.1 Size distribution of the isolated vesicles were measured by DLS

Fractions of exosomes derived from human plasma were isolated by SEC and characterized by DLS (Figure 3.1). DLS was applied to determine the size and homogeneity of vesicles in the isolated fractions. From the vesicles isolated, 50 μL of the sample resuspended in 1x PBS were poured into a quartz cuvette and the sample intensity was read by three reading per sample at room temperature by a Zetasizer Nano S instrument. The intensity of scattered light from the samples was measured and the results were given as diameter of vesicles in nm. Exosomes were

expected to be in a size range 30-100 nm (introduction, 1.5.1), and all fractions of vesicles contained particles in the same size range: F10: 78.97 ± 0.25 d.nm, F11: 58.51 ± 0.36 d.nm, F12: 49.5 ± 0.29 d.nm, F13: 43.06 ± 0.18 d.nm (figure 3.1 and table 3.1) . These values were the average particle diameters of peaks in each size distribution. The presence of one peak for each fraction observed in the figure and low PDI-values (< 0.4) demonstrated homogeneity of the vesicles in the fractions expected to contain exosomes (table 3.1). The next level of evidence for the successful isolation of exosomes was performed by identification of the exosome marker, HSP70, using western blotting.

Table 3.1. PDI-values and z-averages of the selected fractions.

Fraction	Z-averages (d.nm)	PDI-values
F10	78.97 ± 0.25	0.209 ± 0.0105
F11	58.51 ± 0.36	0.205 ± 0.0079
F12	49.5 ± 0.29	0.189 ± 0.007
F13	43.06 ± 0.18	0.21 ± 0.0032

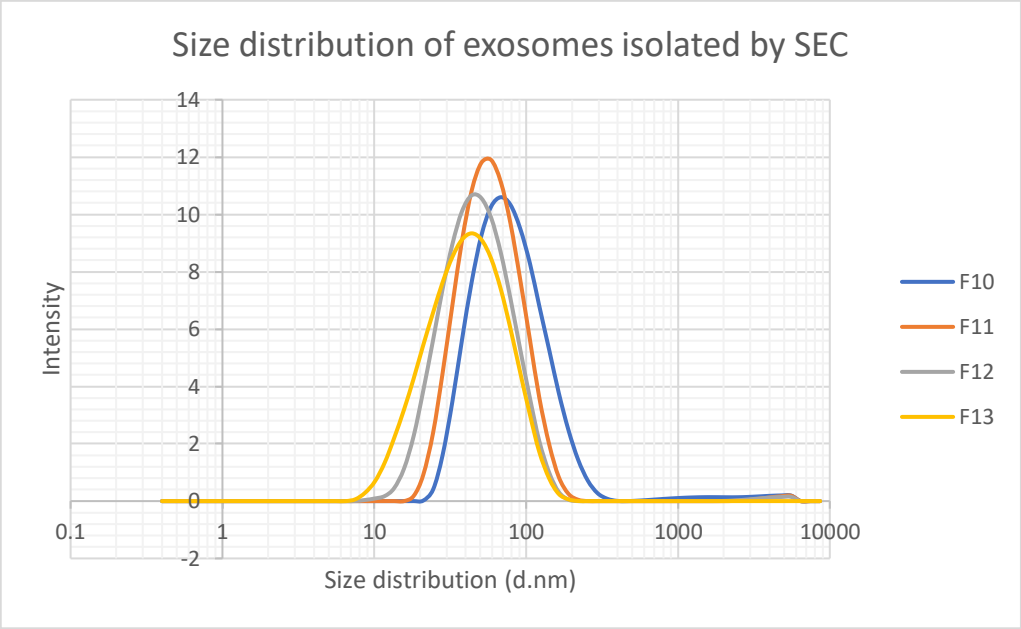

Figure. 3.1. Relative intensity of scattered light versus size distribution of different vesicle fractions isolated by SEC.

3.1.2 Vesicles were characterized by gel electrophoresis and western blotting

DLS analysis and protein quantification were performed prior to separation on a native PAGE gel electrophoresis to determine the suitable fractions of isolated vesicles. Further, the protein concentration in the sample was quantified by the BCA method (methods, section 2.2.5). The estimated concentrations of proteins in the selected fraction were shown in table 3.2.

Table 3.2. Estimated protein concentrations in isolated exosomes measured at 562 nm.

Fractions	**F10**	**F11**	**F12**	**F13**
Quantified concentrations (μg/μl)	0.469	1.142	1.715	2.098

Gel electrophoresis and western blotting were applied to determine the presence of exosome protein markers in the isolated vesicles. Gel electrophoresis followed by Coomassie staining visualized the proteins based on their size and was not specific for the proteins of interest. Western blotting, also known as immunoblotting, was performed for more accurate characterization of exosome protein markers and detection of HSP70.

Coomassie staining and western blotting were performed separately on distinct gels containing some fractions of isolations. The proteins on the gel picked up for Coomassie staining were stained and visualized with a white light scanner (Figure 3.2, a). The signals at about 53 kDa that were expected to represent HSP70 protein were detected in all fractions, but strongest in fraction 13 that matched with the results from protein quantification (table 3.2). Thereafter, the HSP70 signal in the western blotting analysis (figure 3.2, b and c) confirmed the presence of exosome protein marker in the isolated samples, as the primary antibody anti-HSP70 was used. Lack of signals in the other bands with the same size would be because of the low concentrations in the other fractions.

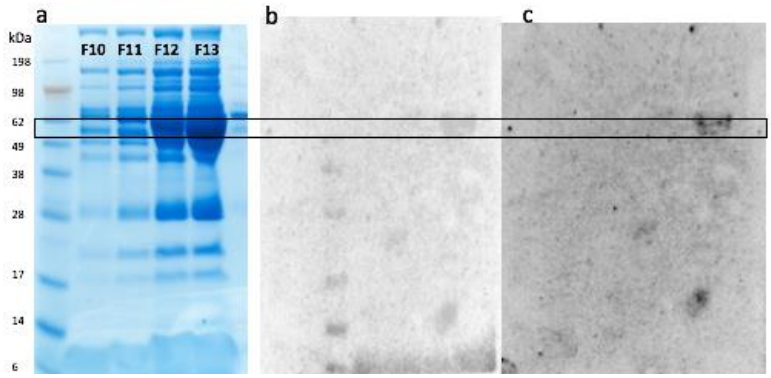

Figure 3.2. Coomassie staining of native PAGE MES gel (a), membrane scanning with standard signal (b) and membrane scanning without standard signal (c).

Next, to improve the visibility of the bands in the gels, the isolated fractions were treated with up-concentrating by filtration in a 100K Amicon filter column or lysed by 2x Radio-immunoprecipitation assay (RIPA) buffer to open the vesicle membranes (described in methods section 2.2.6). In filtration, the concentration factor is dependent on the centrifugation time (table 2.7). The fractions were 26x concentrated prior to separation by electrophoresis. Up-concentration of the vesicles removed the excess proteins and resulted in more distinct bands, while the bands that seemed to contain the protein of our interest were still there (figure 3.3, a).

The other treatment was lysing the sample by 2x RIPA buffer to opening the exosome membrane and accessing to the pure protein as exosome markers. Lysation of the isolated fractions in 2x RIPA buffer improved the visibility of the bands containing the proteins (figure 3.3, b). The combination of up-concentrating and lysation and only up-concentrating did not show significant differences in the protein content and clarity of the bands (figure 3.3, bands N-1x, L-1x, N-26x, and L-26x). Despite the bands at 53-70 kDa that were expected to belong to HSP70, were showed in this figure, concentrating and lysing of the exosome samples could result to missing or degrading of the protein markers and hence no signals were shown in the western blotting of those gels (not showed).

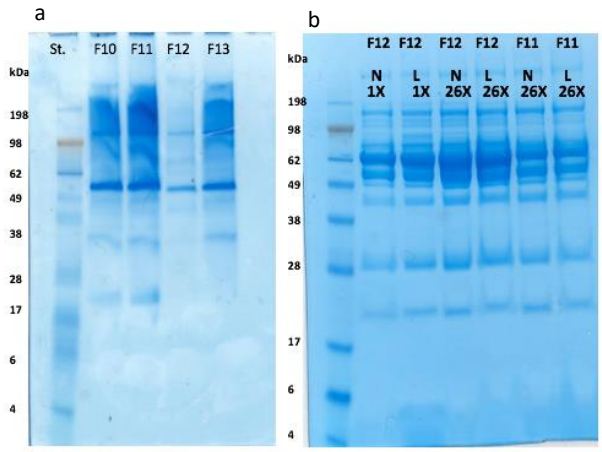

Figure 3.3. Coomassie stained gels containing exosome samples treated with lysing by 2x RIPA buffer (b) and concentrating (a). The selected fractions were concentrated 26x and many unwanted proteins were removed (a). In another experiment (b), to different fractions of exosomes were lysed by 2xRIPA buffer (L) and concentrated (26x) and some of them were only concentrated without lysing (N). L= Lysed, N=Not lysed. 26x= concentrated, 1x= Not concentrated.

To sum up, the small size-ranges observed in DLS data suggested that the isolated vesicles might be exosomes and rather than other EVs that are in the size-range 100-1000 nm (Tamkovich et al., 2016). HSP70 (53-70 kDa) is one of the most characteristics proteins in exosomes that have frequently been used for identification of exosomes (Tamkovich et al., 2016). Incorporation of results obtained from DLS (figure 3.1), protein quantification (table 3.2) and bands observed in the Coomassie stained gel (figure 3.2, a) suggested that the signal in the membrane might belong to the HSP70, the membrane protein of exosomes. Hence, it was assumed that the isolated vesicles might be exosomes, and further analysis were done based on this assumption.

3.2 The standard temperature to store the exosome samples on for some days after isolation were room temperature or 4°C

Maintenance and stability of exosomes in their original biological state is an important issue for truthful analysis of exosome function (Maroto et al., 2017). Standard methods for preservation of exosome samples would be identified prior to further analysis. In this study, the effect of temperature on exosome size and homogeneity reflecting the preservation of exosomes at different temperatures was examined. For this purpose, vesicles were isolated from plasma by SEC and three selected fractions resuspended in 1x PBS were divided in four parts and

stored at three different temperatures; room temperature, 4°C and - 20°C. The size distribution for the stored exosome fractions at different temperatures were measured by DLS.

Freshly prepared fraction of vesicles showed a homogenous size distribution with average sizes of F9 = 48.03 ± 0.21 d.nm, F10 = 40.69 ± 0.24 d.nm, and F11 = 32.92 ± 0.51 d.nm (figure 3.4, a and table 3.3). Measurements three days post isolation revealed no changes in the average size of distribution of exosome fractions stored at room temperature and 4°C (figure 3.4, b and c), while both the z-averages and size distributions were altered in the fractions stored at - 20°C (figure 3.4, d). As shown in table 3.3, z-average for F9 stored at -20°C changed from 48.03 ± 0.21 d.nm to 76.58 ± 0.31 d.nm, and PDI-value for this fraction increased from 0.1696 ± 0.115 to 0.335 ± 0.041. Even after seven days, size averages in the fractions stored at room temperature were nearly similar to the freshly prepared samples (figure 3.4, e). In the samples stored at 4°C, negligible shifts were observed in size averages and PDI-values (figure 3.4, f and table 3.3). In contrast, measurements of DLS data form fractions stores at - 20°C showed changes in both the size distributions and homogeneity of exosomes (figure 3.4, g). Z-averages of exosomes stored at this temperature shifted to F9 = 80.83 ± 2.25 d.nm, F10 = 48.13 ± 78 d.nm, F11 = 41.28 ± 41 d.nm. These measurements indicated that the best condition for storage of vesicles resuspended in PBS for a short time after isolation (until one week) was room temperature, while they showed less stability in - 20°C storages and after repeated freezing-thawing.

Table 3.3. Z-averages and PDI-values for fractions of vesicles selected for determination of a standard for storage of isolated exosomes (first experiment).

Fractions immediately after isolation		
Fractions	**Z-averages (d.nm)**	**PDI-values**
F9	48.03 ± 0.21	0.1696 ± 0.0115
F10	40.69 ± 0.24	0.2496 ± 0.0058
F11	32.92 ± 0.51	0.3053 ± 0.0301
Day 3, fractions stored at room temperature		
Fractions	**Z-averages (d.nm)**	**PDI-values**
F9	49.16 ±0.43	0.262 ± 0.0058
F10	39.02 ±0.21	0.218 ± 0.0051
F11	32.02 ±0.14	0.257 ± 0.0045
Day 3, fractions stored at 4°C		
Fractions	**Z-averages (d.nm)**	**PDI-values**
F9	50.84 ± 0.86	0.237 ± 0.0128
F10	38.74 ± 0.14	0.209 ± 0.0065
F11	33.39 ± 0.09	0.264 ± 0.0040
Day 3, fractions stored at - 20°C		
Fractions	**Z-averages (d.nm)**	**PDI-values**
F9	76.58 ± 0.31	0.335 ± 0.041
F10	43.19 ± 0.16	0.234 ± 0.0037
F11	34.42 ± 0.2	0.279 ± 0.0032
Day 7, fractions stored at room temperature		
Fractions	**Z-averages (d.nm)**	**PDI-values**
F9	48.6 ± 0.59	0.232 ± 0.0227
F10	38.74 ± 0.15	0.195 ± 0.0055
F11	31.17 ± 0.05	0.251 ± 0.004
Day 7, fractions stored at 4°C		
Fractions	**Z-averages (d.nm)**	**PDI-values**
F9	52.28 ± 0.99	0.313 ± 0.021
F10	40.06 ± 1.17	0.231 ± 0.081
F11	33.36 ± 0.41	0.265 ± 0.005
fractions stored at - 20°C		
Fractions	**Z-averages (d.nm)**	**PDI-values**
F9	80.83 ± 2.25	0.277 ± 0.0623
F10	48.13 ± 0.78	0.273 ± 0.002
F11	41.28 ± 0.41	0.512 ± 0.019

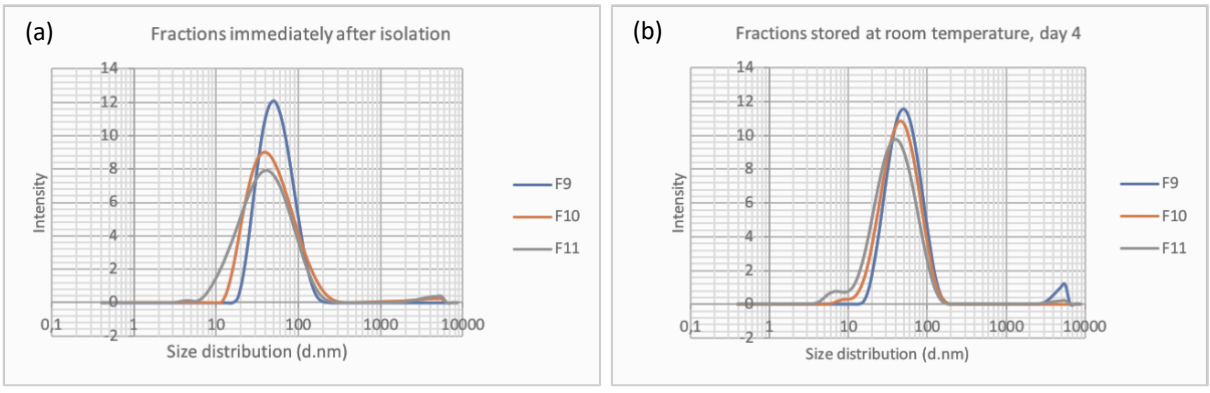

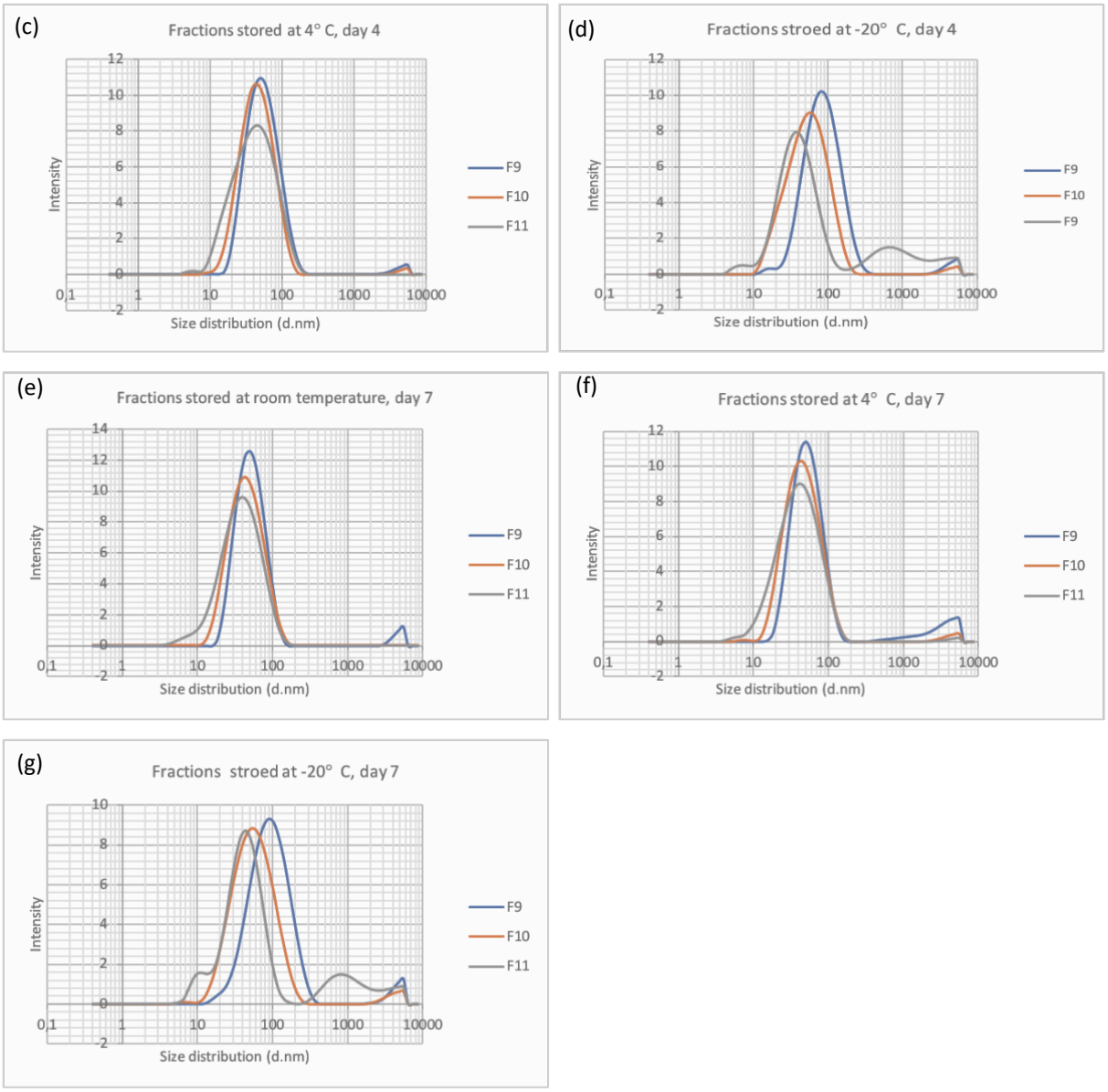

Figure 3.4. Comparison between DLS analysis of fractions immediately after isolation and the fractions stored at different temperatures four- and seven-days post isolation. Size distributions of vesicles immediately after isolation (a), stored at room temperature four days post isolation (b), stored at 4 ℃, four days post isolation (c), stored at - 20 ℃ four days after isolation (d), stored at room temperature seven days after isolation (e), stored at 4 ℃ seven days after isolation (f) and stored at – 20 seven days after isolation (g). All DLS measurements were performed at room temperature on exosomes dissolved in 1x PBS by Malvern Nano ZS instrument using quartz cuvettes, and data were analyzed by a Zetasizer software (version 7.12).

Next, another experiment with the same goal was performed. To determine whether the different storage conditions affected the exosome protein and lipid content, absorbance of prepared samples was measured at 498 nm and 280 nm in addition to DLS measurements simultaneously. One fraction containing vesicles in exosomal size range (F9 = 94.54 d.nm) was divided into four parts, and each fraction was stored at specified temperatures; Room

temperature, 4°C, - 20°C and -80°C. Then, the DLS and absorbance measurements were performed on freshly isolated exosomes, one and five days after isolation.

To evaluate the effect of different storage conditions on lipid and protein content of exosomes, absorption measurements at two different wavelengths was performed. Aromatic amino acids tyrosine and tryptophan present in proteins display ultraviolet absorbance at 280 nm (Noble & Bailey, 2009). Absorbance of lipids making the membrane of exosomes were measured at 498 nm. For absorbance measurements, the isolated fractions were diluted in 1x PBS in a ratio of 1:20, and absorbance was measured at mentioned wavelengths. For each fraction, three measurements were done, and averages of the data were collected to make the diagrams in figure 3.5. Absorbance measured at 280 nm showed the protein content of the exosome fractions (figure 3.5, a), while absorbance measured at 498 nm belonged the lipid content of the exosomes (figure 3.5, b). The absorbance at 280 nm was 0,067, and this value was 0,035 at 498 nm for freshly isolated exosomes. After two days, the absorbances at 280 nm shifted to about 0,076 for samples stored at room temperature, - 20°C and - 80°C, but the shift was less for samples stored on 4°C (0,068). Absorbance at 498 nm did not show significant changes after two days. Five days after isolation, significant alterations were observed in absorbances both at 280 nm and 498 nm for all storage conditions. The exception was absorbance related to lipid content (at 498 nm) in the fraction stored at room temperature that did not show any shift compared to the freshly prepared sample. Also, in these measurements - 20°C storage showed the most alteration, while it seemed that the protein content of vesicles was most stable at room temperature (figure 3.5, b).

(a) (b)

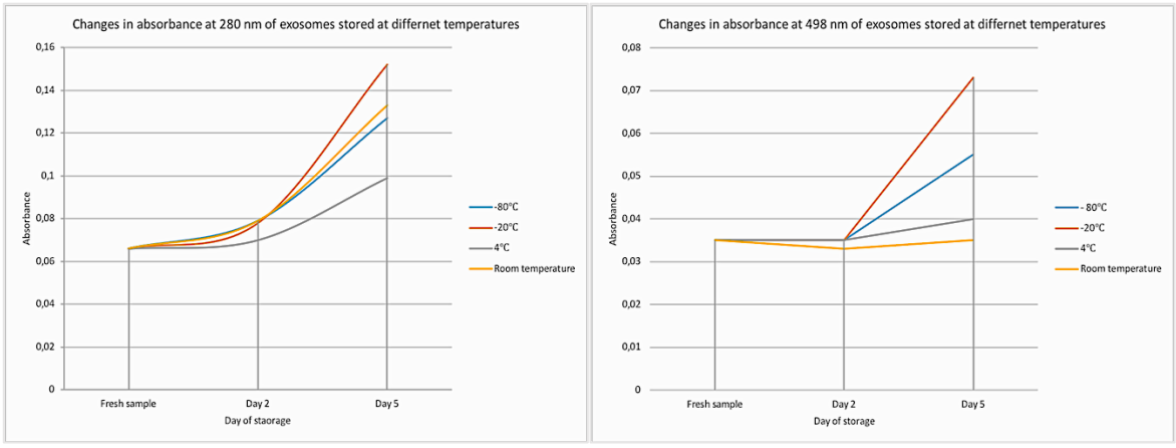

Figure 3.5. Absorbance measurements at 280 nm(a) and 498 nm (b) two and five days post isolation.

To sum up, increase in both lipids and protein contents of exosomes was observed after five days of storage. Most rise were detected on storage at - 20°C, while lipids showed stability at room temperature more than other temperatures.

DLS measurements in the same experiment supported results achieved by absorbance measurements. The freshly prepared sample showed a relatively symmetric size distribution with a size average on 94.54 ± 0.26 d.nm and a PDI-value of 0.2333 ± 0.0032 (table 3.4). This values shifted respectively to 111.83 ± 3.2 d.nm and 0.25 ± 0.0054 in - 20° C storage, and to 122.34 ± 0.43 d.nm and 0.264 ± 0.0063 in - 80°C storage, while not significant shift was observed at room temperature and 4°C storages two days after isolation (figure 3.6, b, c, d and e and table 3.4). After five days of storage, both size distributions and z-averages were altered at - 20°C and - 80°C storages (figure 3.6, h and i). In contrast, size distributions, size values and homogeneity were approximately unchanged for fractions stored at room temperature and 4°C (figure 3.6, f and g). Observations in both experiments with both DLS and absorbance measurements indicated that freezing and thawing formed a population of nanoparticles with larger size averages, increased PDI-values and less homogeneity.

Table. 3.4. Z-averages and PDI-values for fractions isolated for determination of standard temperature for storage (experiment two).

Immediately after isolation	**Z- average (d.nm)**	**PDI-value**
	94.54 ± 0.26	0.2333 ± 0.0032
2 days after isolation		
Temperature	**Z- averages**	**PDI-values**
Room temperature	94.11 ± 0.31	0.224 ± 0.007
4°C	94.15 ± 0.26	0.222 ± 0.005
- 20°C	111.83 ± 3.2	0.25 ± 0.0045
- 80°C	122.34 ± 0.43	0.264 ± 0.0063
5 days after isolation		
Temperature	**Z- average**	**Std. Dev**
Room temperature	99.47 ± 0.58	0.23 ± 0.0127
4°C	102.03 ± 0.64	0.248 ± 0.0051
- 20°C	722.63 ± 5.801	0.961 ± 0.067
- 80°C	156.43 ± 8.53	0.522 ± 0,088

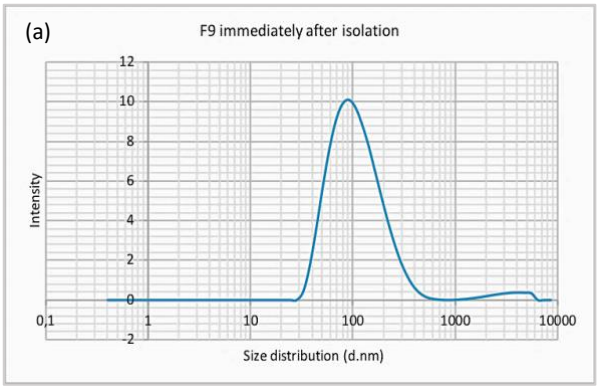
(a)
F9 immediately after isolation
Intensity
Size distribution (d.nm)

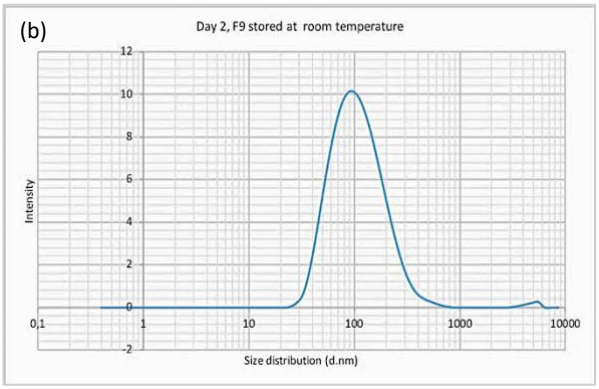
(b)
Day 2, F9 stored at room temperature
Intensity
Size distribution (d.nm)

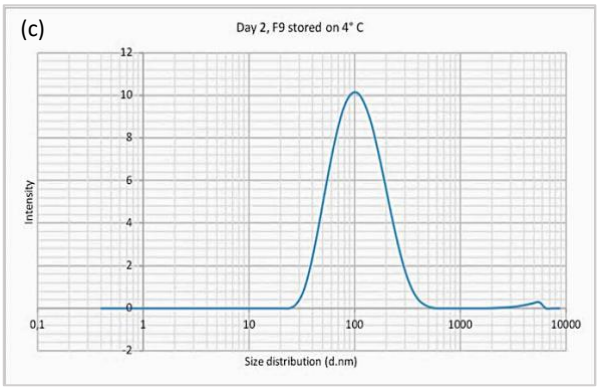
(c)
Day 2, F9 stored on 4° C
Intensity
Size distribution (d.nm)

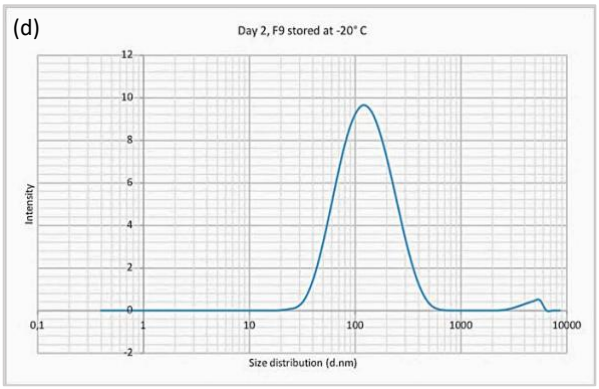
(d)
Day 2, F9 stored at -20° C
Intensity
Size distribution (d.nm)

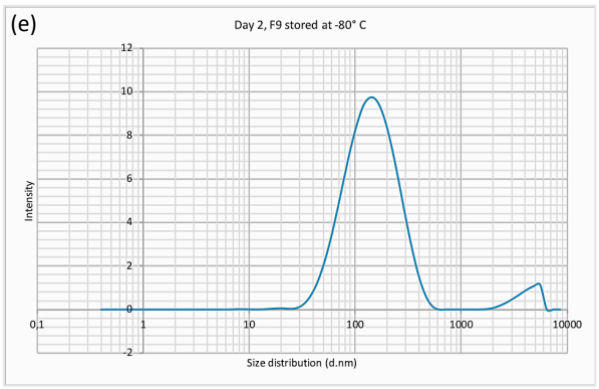
(e)
Day 2, F9 stored at -80° C
Intensity
Size distribution (d.nm)

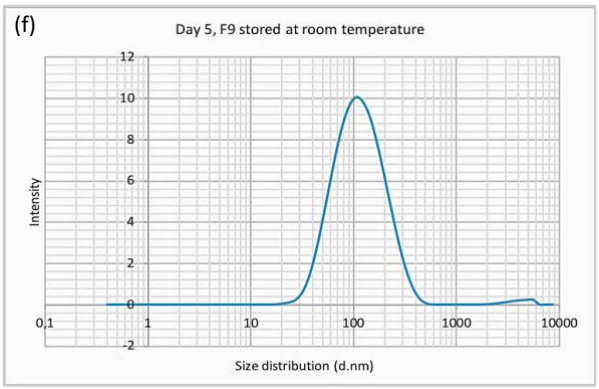
(f)
Day 5, F9 stored at room temperature
Intensity
Size distribution (d.nm)

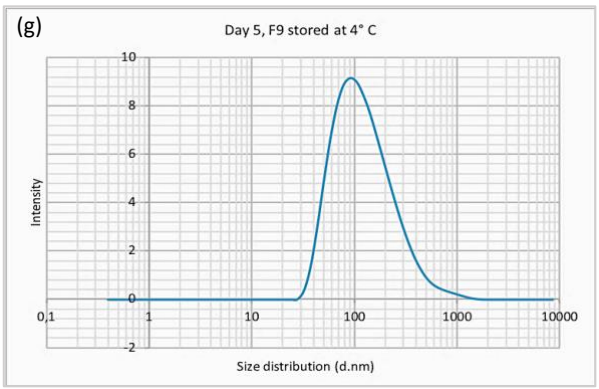
(g)
Day 5, F9 stored at 4° C
Intensity
Size distribution (d.nm)

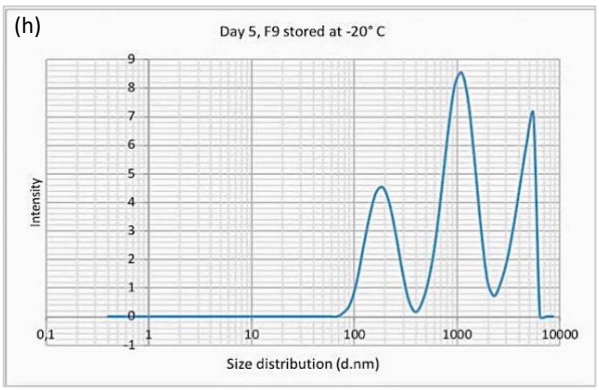
(h)
Day 5, F9 stored at -20° C
Intensity
Size distribution (d.nm)

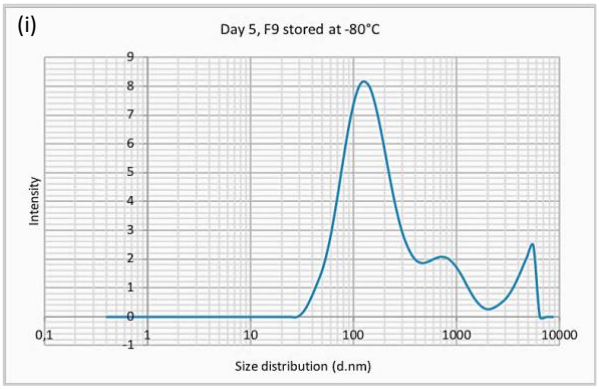

Figure 3.6. DLS measurements showing the comparison between size distribution, size average and homogeneity of the freshly isolated exosome fractions and exosome samples stored in different storage conditions. Freshly prepared F9 (a), F9 stored at room temperature two days post isolation (b), F9 stored at 4℃ two days post isolation (c), F9 stored at - 20℃ two days post isolation (d), F9 stored at -80℃ two days post isolation (e), F9 stored at room temperature five days post isolation (f), F9 stored at 4℃ five days post isolation (g), F9 stored at -20℃ five days post isolation (h), F9 stored at -80℃ five days post isolation (i).

3.3 Exosomes were visualized using confocal microscopy

To assess whether we are able to detect the exosomes with confocal microscopy, they were labeled with RNA-labeling dye, Hoechst. Vesicles determined as exosomes with a size average of 68.45 ± 0.25 nm was selected for the analysis and centrifuged at 16,000 xg for 60 min. at 4°C to pellet the exosomes. The pellet was stained with Hoechst dye (Ex/Em: 350/461 nm) and fixed on a pre-coated coverslip. Confocal imaging was performed with an A1R confocal laser microscope system. The images demonstrated that the RNAs of exosomes were labeled with the Hoechst stain. Both single and clusters of 2-5 exosomes were detected (figure 3.7). It was assumed that detection of exosomes was possible by the available instrument and hence, further analysis to study internalization of exosomes in the hCMEC/D3 cell lines was performed.

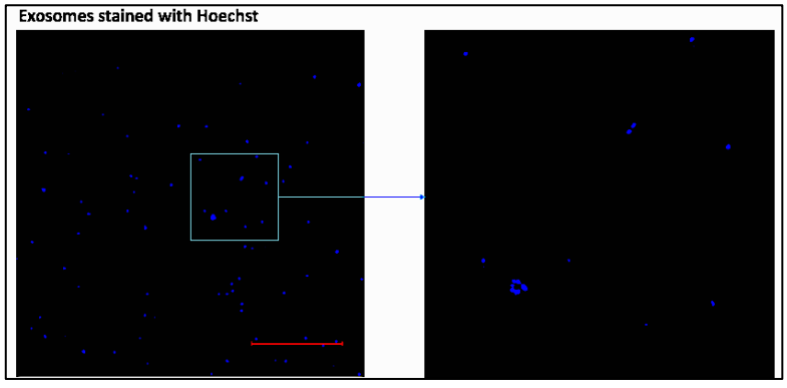

Figure 3.7. Confocal microscopy images of exosome fractions isolated from plasma stained with Hoechst dye, scale bare: 50 µm. Images were taken with assistance of Jodi Maple Grødem at UiS by an A1R confocal laser microscope system.

3.4 Uptake of exosomes isolated from human plasma were by hCMEC/D3 cells was evaluated

Uptake of isolated exosomes originating from human plasma into hCMEC/D3 cells lines as an *in vitro* BBB model was investigated. Isolated exosomes were labeled with WGA 488 (Ex/Em: 490/515). Approximately 18450 cells/cm^2 from passage 4 were cultivated on the sterile coverslips that were pre-coated with collagen (methods, section. 2.2.7.4). When the cells were about 80% confluent (figure 2.2, b), the cells were stained with WGA 640 dye (Ex/Em: 642/662 nm). Then, the pre-stained exosomes were added to the cells and incubated at room temperature for 15 and 30 min. prior to washing them with HBSS and fixing with 4% PFA. Uptake of exosomes by hCMEC/D3 cells was assessed using confocal microscopy.

The confocal analysis of exosomes labeled with WGA 488 showed small green spots with nearly the same sizes readily distinguishable from the background noise (figure 3.8, a, exosomes). These spots were not observable on the negative control even with very high background color (figure 3.8, a, negative control). The image taken from only cells showed elongated red membranes (labeled with WGA 640) surrounding oval blue nucleus (labelled with DAPI) (figure. 3.8, a, only cells).

Next, a representative image of cells incubated with exosomes suggested uptake of exosomes by hCMEC/D3 cells (figure 3.8, b). Channels were separated to view the different channels of the image, and exosomes on the cells were introduced by white arrows (figure 3.8, b). Furthermore, intercellular localization of exosomes in the cells were evaluated by taking images from different layers of specimen and performing 3D visualization. Different dimensions form several locations were visualized (figure 3.8, c and d, figure 7.2). The 3D-images and enlargement areas of the distinct layers showed that the green fluorescent exosomes were located in the same plane as the cells (figure 3.8, c and d), suggesting that the exosomes might have transferred into the cells. However, the obtained images could not show the localization of exosomes according to hCMEC/D3 cells.

(a)

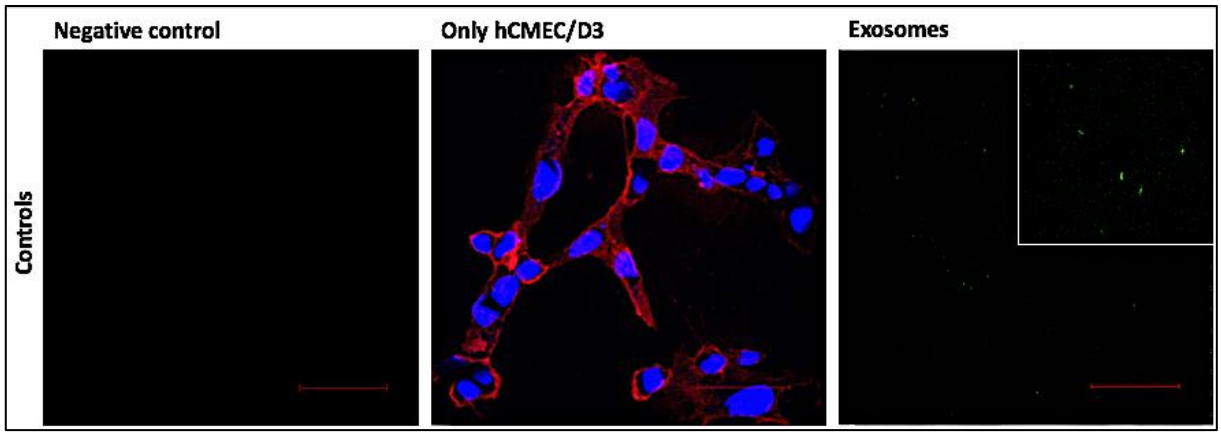
Negative control
Only hCMEC/D3
Exosomes
Controls

(b)

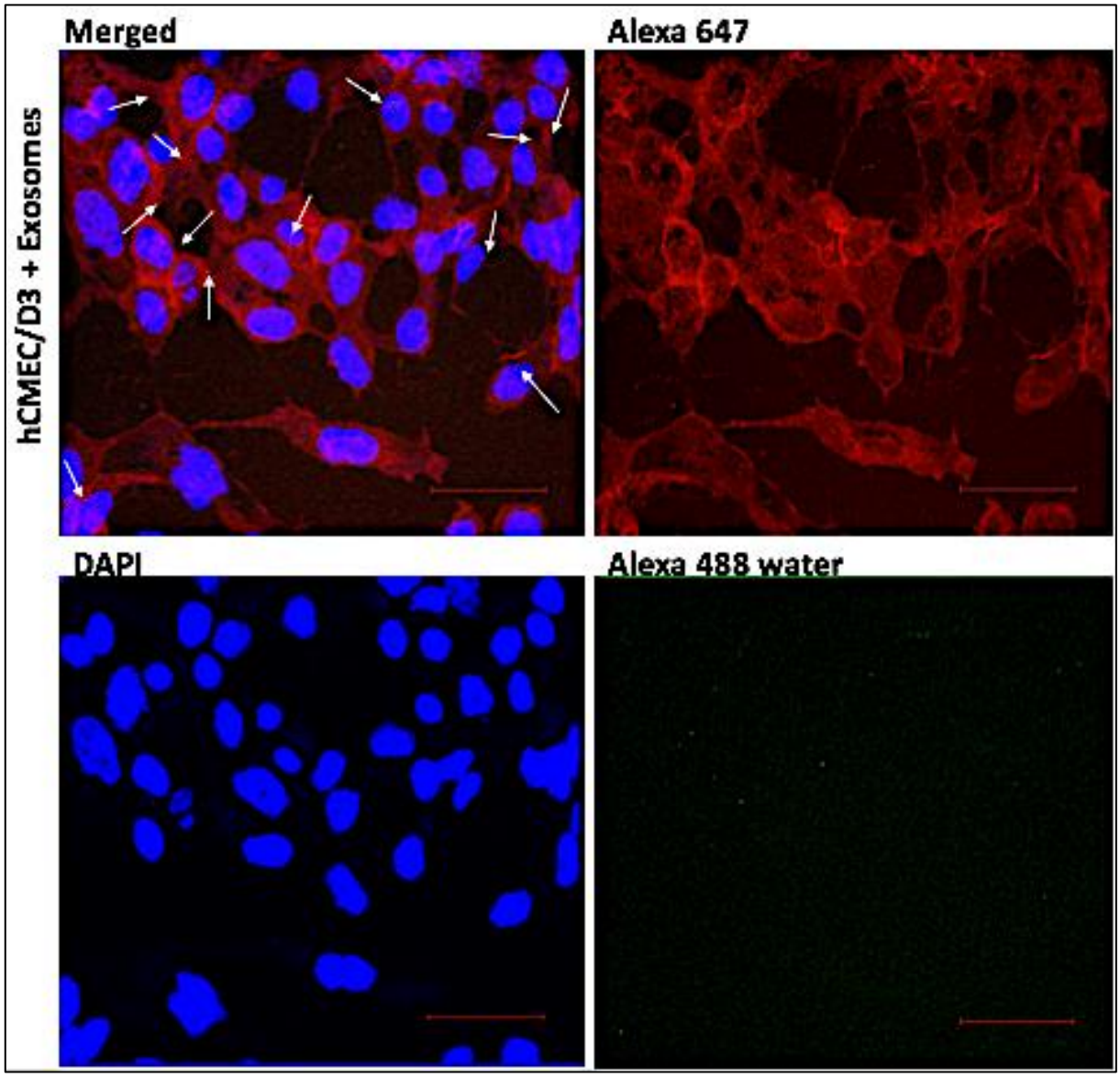
Merged
Alexa 647
hCMEC/D3 + Exosomes
DAPI
Alexa 488 water

(c)

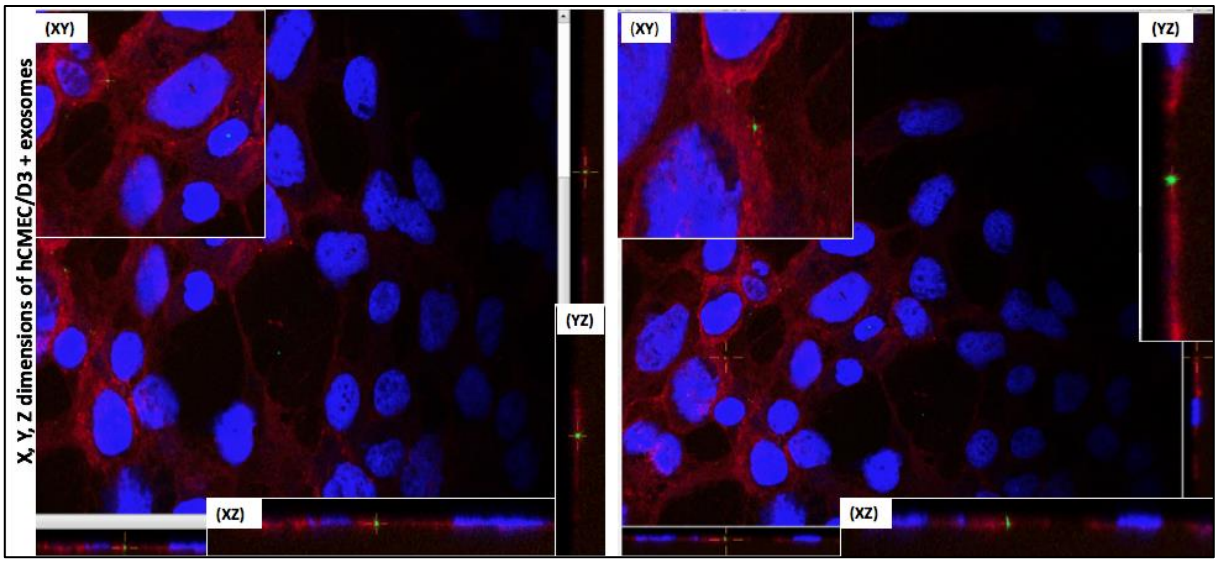

(d)

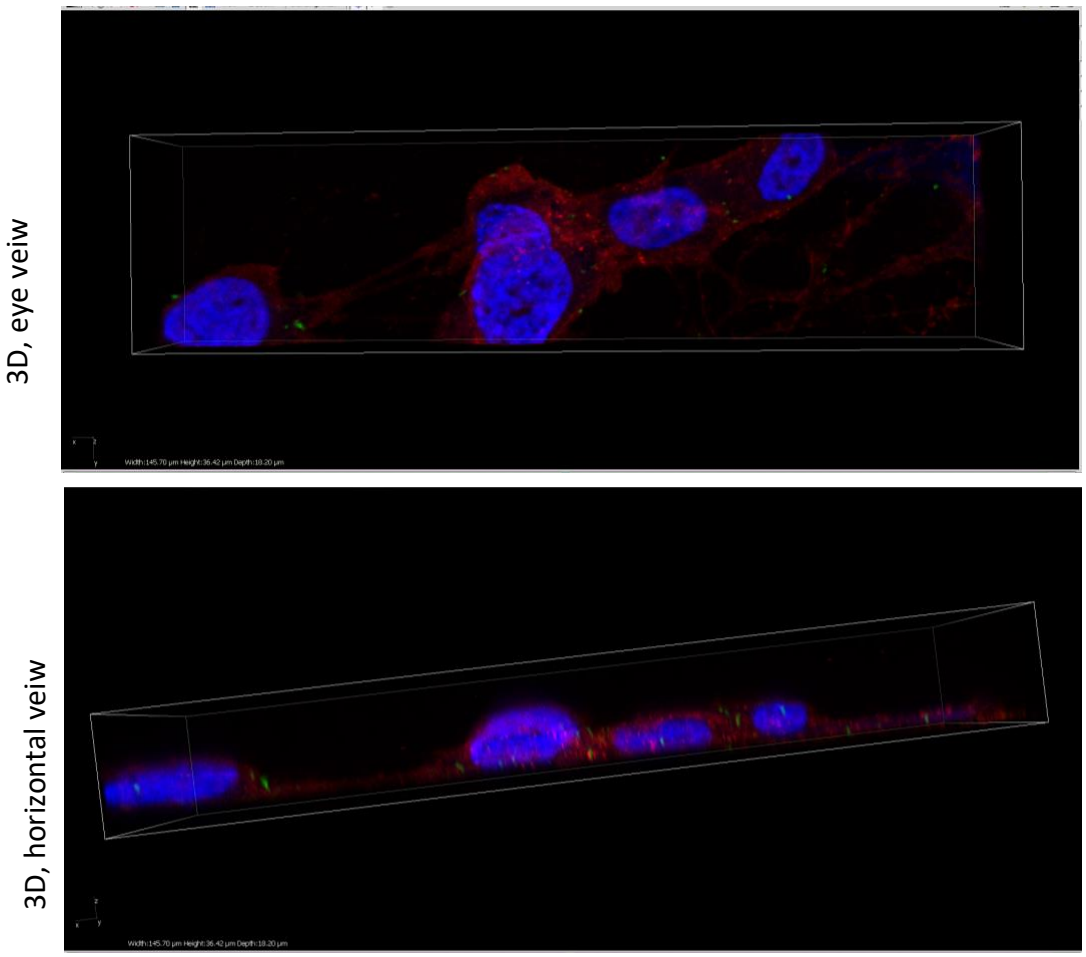

Figure 3.8. Fluorescence confocal microscopy from exosomes uptake by hCMEC/D3. Controls (a), hCMEC/D3 cells added exosomes (b); Exosomes taken up by hCMEC/D3 were shown by white arrows, and separated channels of the same image were performed.; X, Y, Z dimensions of hCMEC/D3 added exosomes (c). 3D-imeges of hCMEC/D3 added exosomes with eye view and horizontal view (d). Scale bare; 50 µm. All images were analyzed by NIS element viewer version 4.40.00. The brightness of images was increased to better seen in printing.

4 Discussions

4.1 Choice of the technique for isolation of plasma derived exosomes

As previously mentioned, several isolation techniques are available to isolate vesicles of interest from different body fluids, and different laboratories employ distinct methods depending on the analysis they want to perform. Plasma is a complex body fluid containing exosomes form different origins due to presence of various cells in the blood (Kalra et al., 2013). Therefore, selection of a suitable isolation technique to obtain a pure exosome sample from plasma is a challenging issue. A good method for the isolation of exosomes should discover following criteria: yielding of highly pure sample with minimum contaminations, enriched in exosomal markers as well as releasing exosomes that preserved their biologically functions. SEC is a method that covers the mentioned criteria and supplies isolation of exosomes suitable for several downstream (Hong, Funk, Muller, Boyiadzis, & Whiteside, 2016). Moreover, *Hong et al.* suggested that the plasma isolated by SEC provide exosomes that are morphologically unscathed, presence of contaminating lipo-proteins and immunoglobulins in the fractions are at a minimum, and that the obtained exosomes are able to mediate intercellular communication.

In the current study, SEC (izon science) was utilized to isolate exosomes from human plasma. While the SEC technology was found to be easy to use, several considerations would be taken during the isolation process. As qEV columns are stored at 4°C, it would be equilibrated to room temperature before use. The columns also required pre- and post-cleanup with at least 10 mL of buffer (methods). They could be used up to 5 times according to the manufacturer. After 5 times utilizing, they had to be washed with either 20 ml of 0,1% triton x-100 or 10 mL 0,5 M NaOH buffer and thereafter with 30-50 ml elution buffer. The cost of the exosome isolations performed was low due to the reusability of the SEC columns used. As it was not possible to load more than 2 mL buffer and 0,5-2 mL plasma depending on the column, washing and preparation of larger quanta of exosomes was time-consuming. All works had to be done carefully, because the filter of column should never dry out. Additionally, the void volume might be carefully measured and the tubes collecting fractions switched out every 0.5 mL collection. The overall time required for isolation using qEV columns was approximately two hours. Isolation using qEV columns only allowed a limited amount of plasma to be loaded on the column. It was not simple to use several columns simultaneously. Thus, requirement of

large amounts of exosomes demanded several hours. Compared with other isolation techniques such as ultracentrifugation and ultrafiltration that have large sample capacity and yield large amounts of exosomes (Duijvesz, Luider, Bangma, & Jenster, 2011; P. Li et al., 2017), SEC was more time-consuming.

Nevertheless, the technique offered vesicles with high purity, moderate size distribution and homogeneity (figure 3.1 and table 3.1). All data obtained by DLS showed presence of only one peak for each fraction showing that the variation in size of the vesicles were homogenous. The isolations yielded exosomes of high quality even after more than 10 isolations, reflected by the same high quality and purity as the first isolation. Repeated DLS measurements after several independent isolations from independent plasma harvest during the whole study showed approximately similar results both in size averages and homogeneity of the representative fractions (figure 3.1 versus 7.4).

4.2 Assessing the quality of the vesicles isolated by SEC

DLS is a fast and accurate technique with high sensitivity that is widely used for determination of the particle-size given as the mean value of the hydrodynamic diameter of the particle (z-average) (Chia et al., 2017). In the present study, DLS was used for determining the size and homogeneity of the vesicles isolated by SEC and characterizing them as exosomes.

Performance of measurements with DLS was simple and did not require additional preparation steps. In addition, only 50 μL of sample was required for one measurement, and the sample cloud be reused. DLS gives diameter of particles based on the light scattered by all the particles present in the sample (Bhattacharjee, 2016). Presence of only one peak for each fraction of vesicles gives an estimation of the purity represented by the homogeneity in the vesicle size of the preparation. The diameters of freshly prepared vesicles in all isolations were determined between 30 – 100 d.nm that are consistent with expected size range of exosomes, and correlate with size average of exosomes detected in other studies (Aryani & Denecke, 2016; Barile & Vassalli, 2017). Our DLS analysis revealed moderate PDI-values (< 0,4), and homogenous size distributions that suggested the purity of the exosome fractions. As discussed in section 1.6.3, PDI-values of 0.1-0.4 might indicate to a moderately polydisperse, and hence, high quality of

sample. However, low resolution and inability to determine particle concentration are the limitations with DLS reported by (Chia et al., 2017) that impressed the performed analyses in this study. For determination of vesicle concentrations, protein quantification using BCA kit was performed.

Results from two separately experiments with identical setup indicated that different temperature storages had significant effects on size and content of the exosomes. Our study showed that the best preservation condition for isolated exosomes with SEC might be room temperature or 4°C. Repeated freezing and thawing led to shift of sizes and alterations in homogeneity of the exosomes as well as the total protein and lipid content of the vesicles. By contrast, storage at 4°C and room temperature showed more stability on size and content shift in both DLS and absorbance measurements. Most alterations were observed in – 20°C storage. Similar finding were achieved in another study which showed that freezing resulted in increased size of exosomes (Maroto et al., 2017). One possible explanation of alteration in size and homogeneity of exosomes might be degradation of their proteins and hence, structural disruption of exosomes (Maroto et al., 2017).

UV absorbance is used to give an estimation of the protein concentration. Proteins absorb spectrum around 280 nm frequently by the aromatic amino acids tyrosine and tryptophan (Noble & Bailey, 2009). The absorbance values given for the concentrations of proteins were lower than the values given for lipids. This was reasonable, as the most part of exosomal membrane composes of lipids (Tamkovich et al., 2016). According to the increase in lipid and proteins of exosome, *Maroto et al.* showed similar results, and the group described that the reason might be the dissociation or lysis of the proteins during storage. It is important to note that the data given by absorbance measurements were too small and outspread to be assumed as an accurate and reliable result for determination of alterations in protein and lipid content of exosomes. Therefore, it can only suggest observation of alteration in total content of vesicles. Probable contaminations might affect the results, as the same sample was used several times. Further experiments using better technologies such as mass spectrometry (Maroto et al., 2017) can be alternative to indicate reliability of the obtained results.

4.3 Western blotting

To verify the DLS results which suggested that the isolated vesicles might be exosomes and to identify an exosomal protein marker, HSP70, western blotting was performed. In the gels stained with Coomassie, several bands were detected. However, the only used antibody was anti-HSP70, and detection of other proteins in the gel with higher and lower molecular weight was not performed due to some limitations. The other bands with the same molecular weight was not detected might in the same membrane. Since, the contrast between the color of the reaction product and the membrane itself is poor (Kurien & Scofield, 2006), the signals for other bands with lower protein concentrations may be extinguished.

The validation of HSP70 as an exosome marker itself is an issue. Some groups introduce HSP70 as the most characteristic protein in exosomes (Tamkovich et al., 2016); (Kalra et al., 2013), while the others suggest that the HSP70 protein is present in all EVs and cannot be used specific for identification of exosomes (Kowala et al., 2016). The size average for the fraction containing this protein was determined only 43.06 ± 0.1778 d.nm in DLS measurement (table 3.1). However, the contrast between different studies regarding this protein lead to the assumption that it is not clear that the HSP70 belong to exosome or other EVs. Proposed by *Kalra et al.*, detection of tetraspanins, CD63 (53 kDa) and CD9 (28 kDa), might clarify that the detected HSP70 originate from exosomes or not. The band in the which might contain these to exosome markers, were detected in Coomassie stained gel (figure 3.2, a), but further attempt to identification of them with mass spectrometry remained unsuccessfully due to laboratory equipment limitations.

4.4 Internalization of the plasma-derived exosomes into hCMEC/D3 cell line

Visualization of exosomes is challenging due to their small size (Duijvesz et al., 2011). Furthermore, *Duijvesz* et al. visualized exosomes by electron microscopy and confocal microscopy in a cancer related study. In that study, exosomes were labeled with lipophilic fluorescent dyes in order to visualization by confocal microscopy, and a bead formed by

multiple exosomes were shown. In line with that study, our study showed Hoechst labeled exosomes both singly and multiply (figure 3.7). Hoechst dye labeled only exosomal RNA, and hence, the morphology and diameter of the vesicles were not detected in the current study.

In order to label exosomes, three fractions containing vesicles with diameter of 58.8 ± 0.254 d.nm were combined to obtain a higher concentration and centrifuged at 16000 xg for 1h at 4°C (methods, 2.2.8). The achieved pellet was not observable with eyes, and possibility to miss some numbers of exosomes during washing steps were high. Nevertheless, identification of morphology and determination of accurate size of exosomes by the available system (A1R confocal laser microscope) was restricted. The characterization of exosomes require very high resolution that can be obtained using electron microscopy (Vlassov, Magdaleno, Setterquist, & Conrad, 2012)

Several studies have investigated on discovery of internalization of exosomes into different cell types and the mechanisms behind molecular and cellular exosome uptake (Costa Verdera, Gitz-Francois, Schiffelers, & Vader, 2017; Durak-Kozica, Baster, Kubat, & Stepien, 2018; Franzen et al., 2014; Tian et al., 2013). The present study suggested that plasma originated exosomes were taken up by hCMEC/D3 cells. The possible internalization of exosomes was evident from the accumulation if the green fluorescent spots which are expected to be exosomes in the hCMEC/D3 cells (figure 3.4, b). However, it was not obvious that they have passed the cell membrane, or they were stranded inside the membrane. The possibility of that they cloud be on/above the cells also existed. Exact localization of the exosomes in the cells was not determined by the obtained images.

The detailed mechanisms of internalization and intracellular trafficking of EVs including exosomes are not well understood yet (Costa Verdera et al., 2017; Purushothaman et al., 2016). However, some groups suggested that the internalization of exosomes occur via endocytosis (Franzen et al., 2014; Purushothaman et al., 2016). A recently published study by *Durak-Kozica et al.* showed the uptake of EVs by endothelial cells and furthermore, demonstrated more accurate localization of EVs into in perinuclear region of the target cells by 3D visualization. In line with this finding, the current study suggests that internalization is observed in some numbers of hCMEC cells. Moreover, some cells remained without uptake of EVs, and there are also some spots freely localized in the medium (figure 3.8). Images showed in figure 3.8, b and c represented the results from two replicates and observations of several locations on the same

specimen, also including 15 min. incubation of exosomes with hCMEC/D3 cells. In all cases, about 5-12 cells form totally 20-30 counted cell contained green fluorescent spots.

However, some considerations would be taken relative to that the concentration of exosomes seemed to be low leading to that several cells remained without exosome uptake and. As mentioned previously, significant number of exosomes might be lost during washing steps before and after labeling and led to low counts of visualized exosomes. Another explanation might be short incubation times, and that some of the exosomes were washed off before they were attached to the cells. It is worth pointing out that the incubation time for similar experiments in another studies was up to 24 h which was significantly longer than incubation time (30 min.) in this study (Durak-Kozica et al., 2018; Dutta et al., 2014). Other publication observed increased uptake of labeled exosomes by Bladder cancer cells with longer incubation time (Franzen et al., 2014).

hCMEC/D3 cells as human BBB model are well-known cells which are widely used for different aspects (Eigenmann et al., 2013). As discussed in the introduction, ABC-transporters, MDRs and p-gp are associated with protection of CNS (section 1.3). *Poller et al*. reported indication of these BBB-specific proteins expressed by hCMEC/D3. In the current study the early passages (3-4) of the cell were utilized. The hCMEC/D3 cells were successfully cultured without Pen-Strep until passage 4. Since, some of flasks in passages 3 and 4 were contaminated during practicing, Pen-Strep was used under the main experiments. Overall, hCMEC/D3 cell lines displayed as easy grown cells which could be cultured, trypsinated, freezed and reproduced in simple manner. Images from hCMEC/D3 cells showed elongated monolayers and this was consistent the morphology of these cells indicated in some previous studies (Eigenmann et al., 2013; Weksler et al., 2013).

Besides all these considerations, possibility of exosome uptake by hCMECs was suggested. It was demonstrated that the green fluorescent exosomes were in the same plane as the cells in images provided from vertical in depth (z) dimensions (figure 3.8, c and d). The obtained 3D-images resemblanced to findings by *Durak-Kuzica et al.* (using different dyes) which demonstrated 3D visualization of exosome internalization into human endothelial cells. However, finding the exact localization of exosomes in the cells were more than the capability of this study and required separately experiments.

5 Conclusions

In this study, a combination of several successful characterization techniques has shown that SEC is an easy and reliable method to isolate vesicles. The isolation revealed vesicles with high purity, low PDI-values and homogenous size distributions. Nevertheless, the technique offered low amounts of vesicles per isolation, and isolation with higher yield was found to be time consuming.

The isolated vesicles by SEC had diameters in the expected range for exosomes (30-100 d.nm). Gel electrophoresis showed bands in 53 -70 kDa that was expected to belong to the exosome marker, HSP70 followed by western blotting which suggested the presence of this protein in the expected band. Out from all these findings, it could be assumed that the isolated vesicles were exosomes. However, the exact morphology and size of exosomes was not clear in the obtained confocal microscopy images. Furthermore, as done in another study, electron microscopy could be an preferable alternative for more accurate evaluation of size and shapes of the isolated exosomes (Wu, Deng, & Klinke, 2015).

DLS and absorbance measurements revealed that exosomes preserved their stability in size, homogeneity and the total content at room temperature and at 4°C better than – 20°C and -80°C, and freezing led to increase in diameter, PDI-values and absorbance of lipids and proteins of exosomes. These results pertained to storage until seven days after isolation. Evaluation of storage for longer time such as months was not investigated in this study.

Studying internalization of exosomes into hCMEC/D3 provided this suggestion that exosome uptake by these cells might be possible. Nevertheless, the intracellular localization of exosomes in the cells was remained unclear. Even in the captured 3D images, it was not obvious that the labeled exosomes were located above, in the membrane or inside the cells.

This study was a very early stage of research ongoing on exosomes as nanocarriers for treatment of epilepsy, and investigations on development of strategies for exosome isolation with high throughput and more exact characterization of exosomes as well as improvement of techniques required for this study are under progress.

6 References

Abbott, N. J., Patabendige, A. A., Dolman, D. E., Yusof, S. R., & Begley, D. J. (2010). Structure and function of the blood-brain barrier. *Neurobiol Dis, 37*(1), 13-25. Retrieved from https://www.ncbi.nlm.nih.gov/pubmed/19664713. doi:10.1016/j.nbd.2009.07.030

Alyautdin, R., Khalin, I., Nafeeza, M. I., Haron, M. H., & Kuznetsov, D. (2014). Nanoscale drug delivery systems and the blood-brain barrier. *Int J Nanomedicine, 9*, 795-811. Retrieved from https://www.ncbi.nlm.nih.gov/pubmed/24550672. doi:10.2147/IJN.S52236

Aryani, A., & Denecke, B. (2016). Exosomes as a Nanodelivery System: a Key to the Future of Neuromedicine? *Mol Neurobiol, 53*(2), 818-834. Retrieved from https://www.ncbi.nlm.nih.gov/pubmed/25502465. doi:10.1007/s12035-014-9054-5

Ballabh, P., Braun, A., & Nedergaard, M. (2004). The blood-brain barrier: an overview: structure, regulation, and clinical implications. *Neurobiol Dis, 16*(1), 1-13. Retrieved from https://www.ncbi.nlm.nih.gov/pubmed/15207256. doi:10.1016/j.nbd.2003.12.016

Barile, L., & Vassalli, G. (2017). Exosomes: Therapy delivery tools and biomarkers of diseases. *Pharmacol Ther, 174*, 63-78. Retrieved from https://www.ncbi.nlm.nih.gov/pubmed/28202367. doi:10.1016/j.pharmthera.2017.02.020

Berg, J. M., Tymoczko, J. L., & Stryer, L. (2012). *Biochemistery* (7th ed.): Kate Ahr Parker.

Bhatt, P., & Narvekar, P. (2018). Challenges and strategies for drug transport aross the BBB. *Neuroscience, 3*(3), 17-21. doi:10.20431/2456-057X.0303004

Bhattacharjee, S. (2016). DLS and zeta potential - What they are and what they are not? *J Control Release, 235*, 337-351. Retrieved from https://www.ncbi.nlm.nih.gov/pubmed/27297779. doi:10.1016/j.jconrel.2016.06.017

Boets, S. D. S., Janssens, P., Lavreysen, H., & Steckler, T. (2105). In the grey zone between epilepsy and schizophrenia: alterations in group II metabotropic glutamate receptors. *Springer, 115*(3), 221-132. doi:https://doi.org/10.1007/s13760-014-0407-7

Boing, A. N., van der Pol, E., Grootemaat, A. E., Coumans, F. A., Sturk, A., & Nieuwland, R. (2014). Single-step isolation of extracellular vesicles by size-exclusion chromatography. *J Extracell Vesicles, 3*. Retrieved from https://www.ncbi.nlm.nih.gov/pubmed/25279113. doi:10.3402/jev.v3.23430

Chia, B. S., Low, Y. P., Wang, Q., Li, P., & Gao, Z. (2017). Advances in exosome quantification techniques. *TrAC Trends in Analytical Chemistry, 86*, 93-106. doi:10.1016/j.trac.2016.10.012

Costa Verdera, H., Gitz-Francois, J. J., Schiffelers, R. M., & Vader, P. (2017). Cellular uptake of extracellular vesicles is mediated by clathrin-independent endocytosis and macropinocytosis. *J Control Release, 266*, 100-108. Retrieved from https://www.ncbi.nlm.nih.gov/pubmed/28919558. doi:10.1016/j.jconrel.2017.09.019

Daneman, R., & Prat, A. (2015). The blood-brain barrier. *Cold Spring Harb Perspect Biol, 7*(1), a020412. Retrieved from https://www.ncbi.nlm.nih.gov/pubmed/25561720. doi:10.1101/cshperspect.a020412

Doboszewska, U., Mlyniec, K., Wlaz, A., Poleszak, E., Nowak, G., & Wlaz, P. (2019). Zinc signaling and epilepsy. *Pharmacol Ther, 193*, 156-177. Retrieved from https://www.ncbi.nlm.nih.gov/pubmed/30149099. doi:10.1016/j.pharmthera.2018.08.013

Duijvesz, D., Luider, T., Bangma, C. H., & Jenster, G. (2011). Exosomes as biomarker treasure chests for prostate cancer. *Eur Urol, 59*(5), 823-831. Retrieved from https://www.ncbi.nlm.nih.gov/pubmed/21196075. doi:10.1016/j.eururo.2010.12.031

Durak-Kozica, M., Baster, Z., Kubat, K., & Stepien, E. (2018). 3D visualization of extracellular vesicle uptake by endothelial cells. *Cell Mol Biol Lett, 23*, 57. Retrieved from https://www.ncbi.nlm.nih.gov/pubmed/30574165. doi:10.1186/s11658-018-0123-z

Dutta, S., Warshell, C., Bandypadhyay, C., Dutta, D., & Chandran, B. (2014). Interactions between Exosomes from Breast Cancer Cells and Primary Mammary Epithelial Cells Leads to Generation of Reactive Oxygen Species Which Induce DNA Damage Response, Stabilization of p53 and Autophagy in Epithelial Cells
. *PLOS ONE*. Retrieved from https://doi.org/10.1371/journal.pone.0097580.

Edgar, J. R. (2016). Q&A: What are exosomes, exactly? *BMC Biol, 14*, 46. Retrieved from https://www.ncbi.nlm.nih.gov/pubmed/27296830. doi:10.1186/s12915-016-0268-z

Eigenmann, D. E., Xue, G., Kim, K. S., Moses, A. V., Hamburger, M., & Oufir, M. (2013). Comparative study of four immortalized human brain capillary endothelial cell lines, hCMEC/D3, hBMEC, TY10, and BB19, and optimization of culture conditions, for an in vitro blood–brain
barrier model for drug permeability studies. *Fluids and Barriers of the CNS, 10*(33).

Farooqi, A. A., Desai, N. N., Qureshi, M. Z., Librelotto, D. R. N., Gasparri, M. L., Bishayee, A., . . . Daglia, M. (2018). Exosome biogenesis, bioactivities and functions as new delivery systems of natural compounds. *Biotechnol Adv, 36*(1), 328-334. Retrieved from https://www.ncbi.nlm.nih.gov/pubmed/29248680. doi:10.1016/j.biotechadv.2017.12.010

Franzen, C. A., Simms, P. E., Van Huis, A. F., Foreman, K. E., Kuo, P. C., & Gupta, G. N. (2014). Characterization of uptake and internalization of exosomes by bladder cancer cells. *Biomed Res Int, 2014*, 619829. Retrieved from https://www.ncbi.nlm.nih.gov/pubmed/24575409. doi:10.1155/2014/619829

Giau, V. V., & A.An, S. S. (2016). Emergence of exosomal miRNAs as a diagnostic biomarker for Alzheimer's disease. *Journal of the Neurological Sciences, 360*, 141-152.

Ha, D., Yang, N., & Nadithe, V. (2016). Exosomes as therapeutic drug carriers and delivery vehicles across biological membranes: current perspectives and future challenges. *Acta Pharm Sin B, 6*(4), 287-296. Retrieved from https://www.ncbi.nlm.nih.gov/pubmed/27471669. doi:10.1016/j.apsb.2016.02.001

Haney, M. J., Klyachko, N. L., Zhao, Y., Gupta, R., Plotnikova, E. G., He, Z., . . . Batrakova, E. V. (2015). Exosomes as drug delivery vehicles for Parkinson's disease therapy. *J Control Release, 207*, 18-30. Retrieved from https://www.ncbi.nlm.nih.gov/pubmed/25836593. doi:10.1016/j.jconrel.2015.03.033

Hong, C.-S., Funk, S., Muller, L., Boyiadzis, M., & Whiteside, T. L. (2016). Isolation of biologically active and morphologically intact exosomes from plasma of patients with cancer. *Journal of Extracellular vesicles, 5*(1). doi:10.3402/jev.v5.29289

Hubbard, J. A., & Binder, D. K. (2016). Blood–Brain Barrier Disruption. In *Astrocytes and Epilepsy* (pp. 291-311).

Jefferys, J. G. (2010). Advances in understanding basic mechanisms of epilepsy and seizures. *Seizure, 19*(10), 638-646. Retrieved from https://www.ncbi.nlm.nih.gov/pubmed/21095139. doi:10.1016/j.seizure.2010.10.026

Kalra, H., Adda, C. G., Liem, M., Ang, C. S., Mechler, A., Simpson, R. J., . . . Mathivanan, S. (2013). Comparative proteomics evaluation of plasma exosome isolation techniques and assessment of the stability of exosomes in normal human blood plasma. *Proteomics, 13*(22), 3354-3364. doi: https://doi-org.ezproxy.uis.no/10.1002/pmic.201300282

Kovacs, R., Heinemann, U., & Steinhauser, C. (2012). Mechanisms underlying blood-brain barrier dysfunction in brain pathology and epileptogenesis: role of astroglia. *Epilepsia, 53 Suppl 6*, 53-59. Retrieved from https://www.ncbi.nlm.nih.gov/pubmed/23134496. doi:10.1111/j.1528-1167.2012.03703.x

Kowala, J., Arrasb, G., Colomboa, M., Jouvea, M., Moratha, J. P., Primdal-Bengtsona, B., . . . Théry, C. (2016). Proteomic comparison defines novel markers to
characterize heterogeneous populations of
extracellular vesicle subtypes. *PNAS PLUS*, E968-E977. doi: www.pnas.org/cgi/doi/10.1073/pnas.1521230113

Kurien, B. T., & Scofield, R. H. (2006). Western blotting. *Methods, 38*(4), 283-293. Retrieved from https://www.ncbi.nlm.nih.gov/pubmed/16483794. doi:10.1016/j.ymeth.2005.11.007

Kwan, P., & Brodie, M. J. (2005). Potential role of drug transporters in the patogenesis of medically intractable epilepsy. *46*(2), 224-235.

Li, P., Kaslan, M., Lee, S. H., Yao, J., & Gao, Z. (2017). Progress in Exosome Isolation Techniques. *Theranostics, 7*(3), 789-804. Retrieved from https://www.ncbi.nlm.nih.gov/pubmed/28255367. doi:10.7150/thno.18133

Li, Q., Li, Q. Q., Jia, J. N., Liu, Z. Q., Zhou, H. H., & Mao, X. Y. (2019). Targeting gap junction in epilepsy: Perspectives and challenges. *Biomed Pharmacother, 109*, 57-65. Retrieved from https://www.ncbi.nlm.nih.gov/pubmed/30396092. doi:10.1016/j.biopha.2018.10.068

Loscher, W. (2005). How to explain multidrug resistance in Epilepsy. *Epilepsy currents, 5*, 107-112.

Luan, X., Sansanaphongpricha, K., Myers, I., Chen, H., Yuan, H., & Sun, D. (2017). Engineering exosomes as refined biological nanoplatforms for drug delivery. *Acta Pharmacol Sin, 38*(6), 754-763. Retrieved from https://www.ncbi.nlm.nih.gov/pubmed/28392567. doi:10.1038/aps.2017.12

Mantegazza, M., Curia, G., Biagini, G., Ragsdale, D. S., & Avoli, M. (2010). Voltage-gated sodium channels as therapeutic targets in epilepsy and other neurological disorders. *The Lancet Neurology, 9*(4), 413-424. doi:https://doi.org/10.1016/S1474-4422(10)70059-4

Maroto, R., Zhao, Y., Jamaluddin, M., Popov, V. L., Wang, H., Kalubowilage, M., . . . Brasier, A. R. (2017). Effects of storage temperature on airway exosome integrity for diagnostic and functional analyses. *J Extracell Vesicles, 6*(1), 1359478. Retrieved from https://www.ncbi.nlm.nih.gov/pubmed/28819550. doi:10.1080/20013078.2017.1359478

Niu, X., Chen, J., & Gao, J. (2018). Nanocarriers as a powerful vehicle to overcome blood-brain barrier in treating neurodegenerative diseases: Focus on recent advances. *Asian Journal of Pharmaceutical Sciences*. doi:10.1016/j.ajps.2018.09.005

Noble, J. E., & Bailey, M. J. A. (2009). Quantification of protein. In *Methods in Enzymology* (Vol. 463, pp. 74-91).

Poller, B., Gutmann, H., Krahenbuhl, S., Weksler, B., Romero, I., Couraud, P. O., . . . Huwyler, J. (2008). The human brain endothelial cell line hCMEC/D3 as a human blood-brain barrier model for drug transport studies. *J Neurochem, 107*(5), 1358-1368. Retrieved from https://www.ncbi.nlm.nih.gov/pubmed/19013850.

Price, R. L., & Jerome, W. G. J. (2011a). 3D reconstruction of confocal image data. In *Basic Confocal Microscopy* (pp. 243). School of Medicine, University of South, Carolina
6439 Garner's Ferry Road
Columbia, SC, USA
Department of Pathology
Vanderbilt University Medical Center
U-2206 MCN, 1161 21st Avenue,
South Nashville, TN
USA: Springer.

Price, R. L., & Jerome, W. G. J. (2011b). Fluorescence Microscopy. In *Basic Confocal Microscopy* (pp. 29). School of Medicine, University of South, Carolina
6439 Garner's Ferry Road
Columbia, SC, USA
Department of Pathology
Vanderbilt University Medical Center
U-2206 MCN, 1161 21st Avenue,
South Nashville, TN
USA: Springer.

Price, R. L., & Jerome, W. G. J. (2011c). Introduction and historical perspective. In *Basic Confocal Microscopy* (pp. 1). School of Medicine, University of South, Carolina
6439 Garner's Ferry Road
Columbia, SC, USA
Department of Pathology
Vanderbilt University Medical Center
U-2206 MCN, 1161 21st Avenue,
South Nashville, TN
USA: Springer.

Price, R. L., & Jerome, W. G. J. (2011d). Setting the operating parameters. In *Basic Confocal Microscopy* (pp. 181). School of Medicine, University of South, Carolina
6439 Garner's Ferry Road
Columbia, SC, USA
Department of Pathology
Vanderbilt University Medical Center
U-2206 MCN, 1161 21st Avenue,
South Nashville, TN
USA: Springer.

Price, R. L., & Jerome, W. G. J. (2011e). Specimen preparation. In *Basic Confocal Microscopy* (pp. 61). School of Medicine, University of South, Carolina
6439 Garner's Ferry Road
Columbia, SC, USA
Department of Pathology
Vanderbilt University Medical Center
U-2206 MCN, 1161 21st Avenue,
South Nashville, TN
USA: Springer.

Price, R. L., & Jerome, W. G. J. (2011f). The Theory of Fluorescence. In *Basic Confocal Microscopy* (pp. 17). School of Medicine, University of South, Carolina
6439 Garner's Ferry Road
Columbia, SC, USA
Department of Pathology
Vanderbilt University Medical Center
U-2206 MCN, 1161 21st Avenue,
South Nashville, TN
USA: Springer.

Purushothaman, A., Bandari, S. K., Liu, J., Mobley, J. A., Brown, E. E., & Sanderson, R. D. (2016). Fibronectin on the Surface of Myeloma Cell-derived Exosomes Mediates Exosome-Cell Interactions. *J Biol Chem, 291*(4), 1652-1663. Retrieved from https://www.ncbi.nlm.nih.gov/pubmed/26601950. doi:10.1074/jbc.M115.686295

Soukupova, M., Binaschi, A., Falcicchia, C., Palma, E., Roncon, P., Zucchini, S., & Simonato, M. (2015). Increased extracellular levels of glutamate in the hippocampus of chronically epileptic rats. *Neuroscience, 301*, 246-253. Retrieved from https://www.ncbi.nlm.nih.gov/pubmed/26073699. doi:10.1016/j.neuroscience.2015.06.013

Stranska, R., Gysbrechts, L., Wouters, J., Vermeersch, P., Bloch, K., Dierickx, D., . . . Snoeck, R. (2018). Comparison of membrane affinity-based method with size-exclusion chromatography for isolation of exosome-like vesicles from human plasma. *J Transl Med, 16*(1), 1. Retrieved from https://www.ncbi.nlm.nih.gov/pubmed/29316942. doi:10.1186/s12967-017-1374-6

Tam, V. H., Sosa, C., Liu, R., Yao, N., & Priestley, R. D. (2016). Nanomedicine as a non-invasive strategy for drug delivery across the blood brain barrier. *International Journal of Pharmaceutics, 515*(1), 331-342. doi:https://doi.org/10.1016/j.ijpharm.2016.10.031

Tamkovich, S. N., Tutanov, O. S., & Laktionov, P. P. (2016). Exosomes: Generation, structure, transport, biological activity, and diagnostic application. *Biochemistry (Moscow) Supplement Series A: Membrane and Cell Biology, 10*(3), 163-173. doi:10.1134/s1990747816020112

Teleanu, D. M., Chircov, C., Grumezescu, A. M., & Teleanu, R. I. (2019). Neuronanomedicine: An Up-to-Date Overview. *Pharmaceutics, 11*(3). Retrieved from https://www.ncbi.nlm.nih.gov/pubmed/30813646. doi:10.3390/pharmaceutics11030101

Tian, T., Zhu, Y. L., Hu, F. H., Wang, Y. Y., Huang, N. P., & Xiao, Z. D. (2013). Dynamics of exosome internalization and trafficking. *J Cell Physiol, 228*(7), 1487-1495. Retrieved from https://www.ncbi.nlm.nih.gov/pubmed/23254476. doi:10.1002/jcp.24304

Vlassov, A. V., Magdaleno, S., Setterquist, R., & Conrad, R. (2012). Exosomes: current knowledge of their composition, biological functions, and diagnostic and therapeutic potentials. *Biochim Biophys Acta, 1820*(7), 940-948. Retrieved from https://www.ncbi.nlm.nih.gov/pubmed/22503788. doi:10.1016/j.bbagen.2012.03.017

Weksler, B., Romero, I. A., & Couraud, P. O. (2013). The hCMEC/D3 cell line as a model of the human blood brain barrier. *Fluids Barriers CNS, 10*(1), 16. Retrieved from https://www.ncbi.nlm.nih.gov/pubmed/23531482. doi:10.1186/2045-8118-10-16

Wu, Y., Deng, W., & Klinke, D. J., 2nd. (2015). Exosomes: improved methods to characterize their morphology, RNA content, and surface protein biomarkers. *Analyst, 140*(19), 6631-6642. Retrieved from https://www.ncbi.nlm.nih.gov/pubmed/26332016. doi:10.1039/c5an00688k

Yang, T., Martin, P., Fogarty, B., Brown, A., Schurman, K., Phipps, R., . . . Bai, S. (2015). Exosome delivered anticancer drugs across the blood-brain barrier for brain cancer therapy in Danio rerio. *Pharm Res, 32*(6), 2003-2014. Retrieved from https://www.ncbi.nlm.nih.gov/pubmed/25609010. doi:10.1007/s11095-014-1593-y

7 Appendix

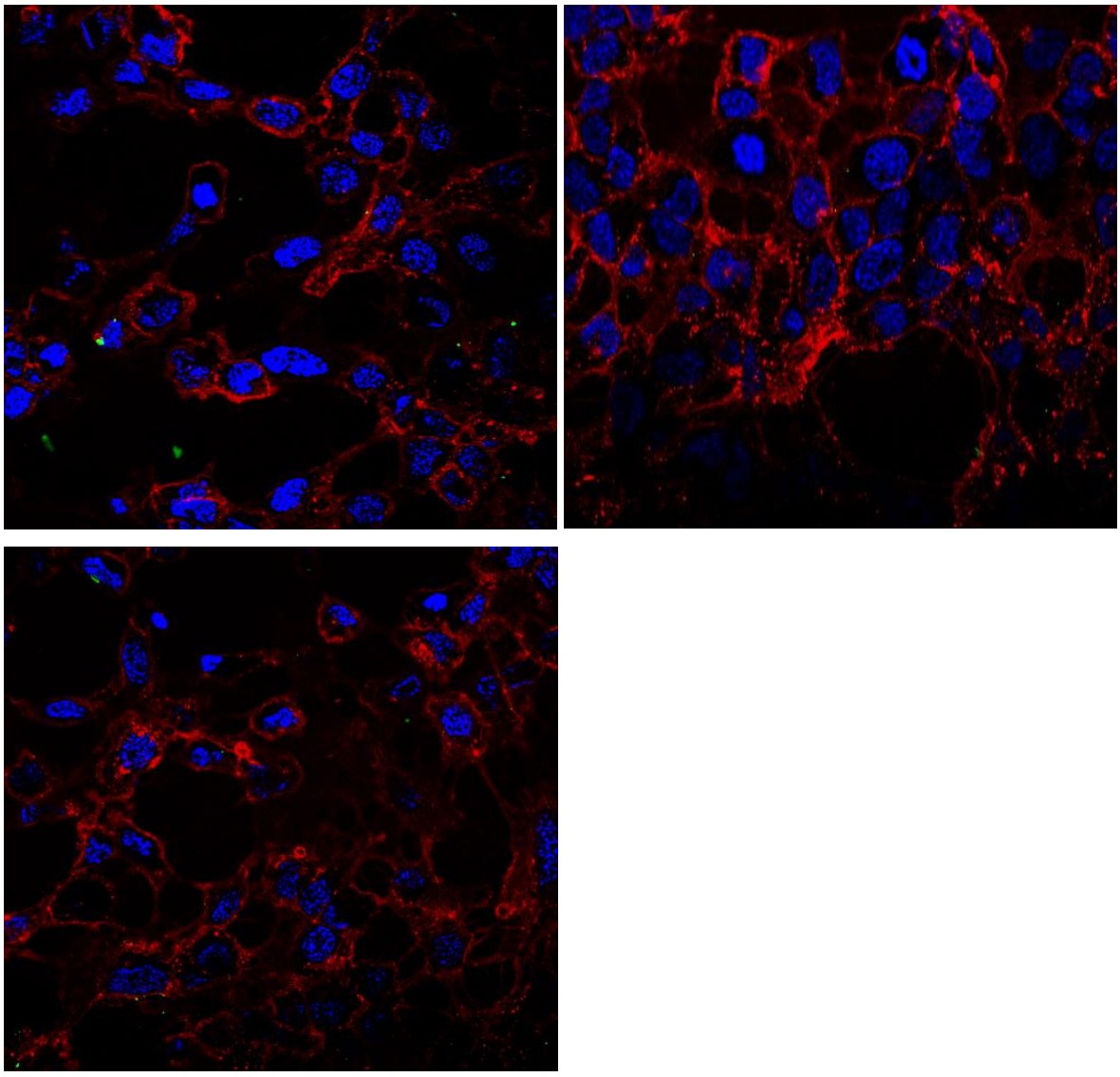

Figure 7.1. Merged 2D view of the hCMEC/D3 cells incubated with exosomes. Distinct images show several specimens prepared as replicates for experiment that was performed for assessing the internalization of exosomes in the cells.

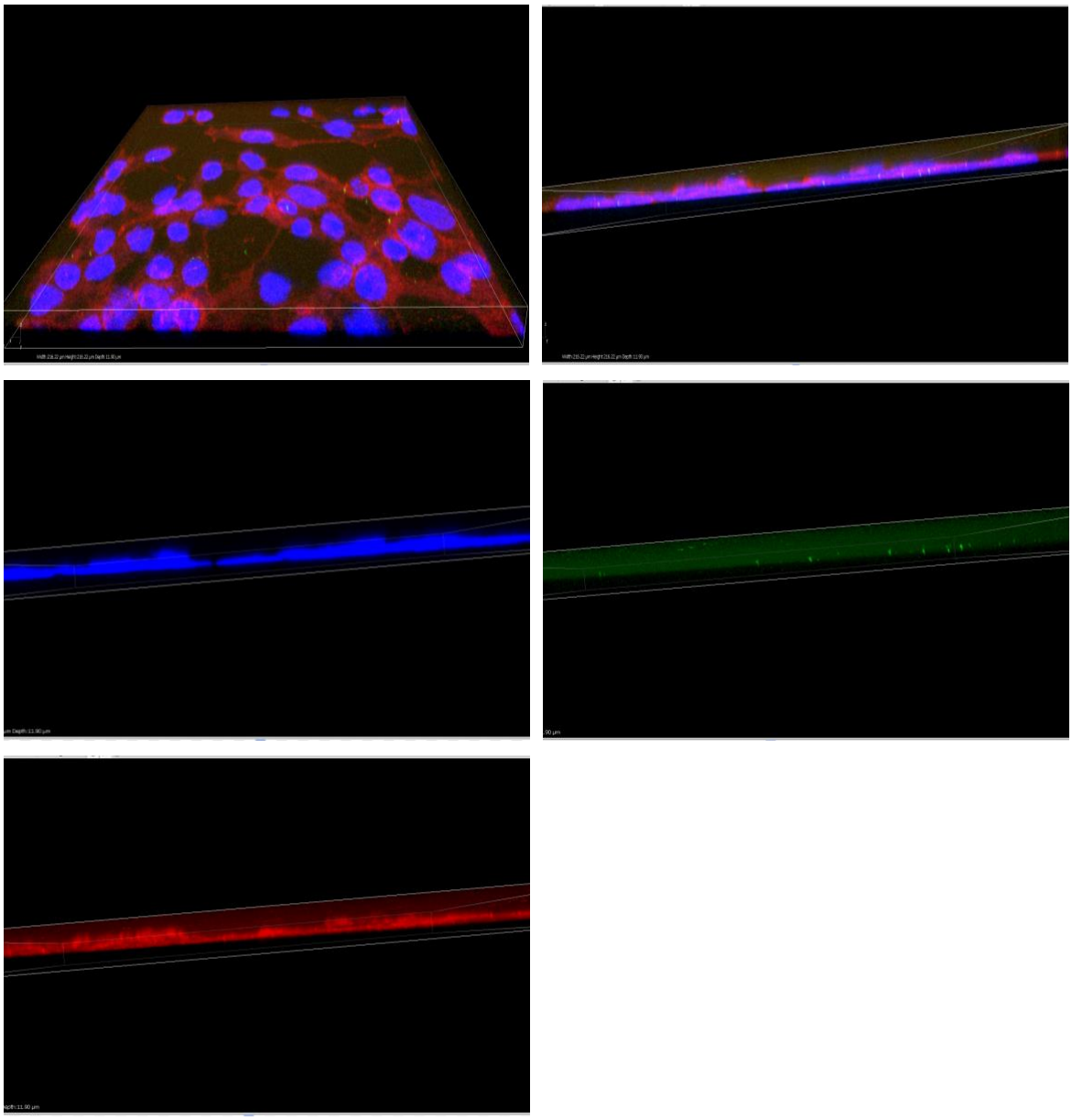

Figure 7.2. Horizontal 3D visualization of merged and separated channels of hCMEC/D3 cells incubated with exosomes.

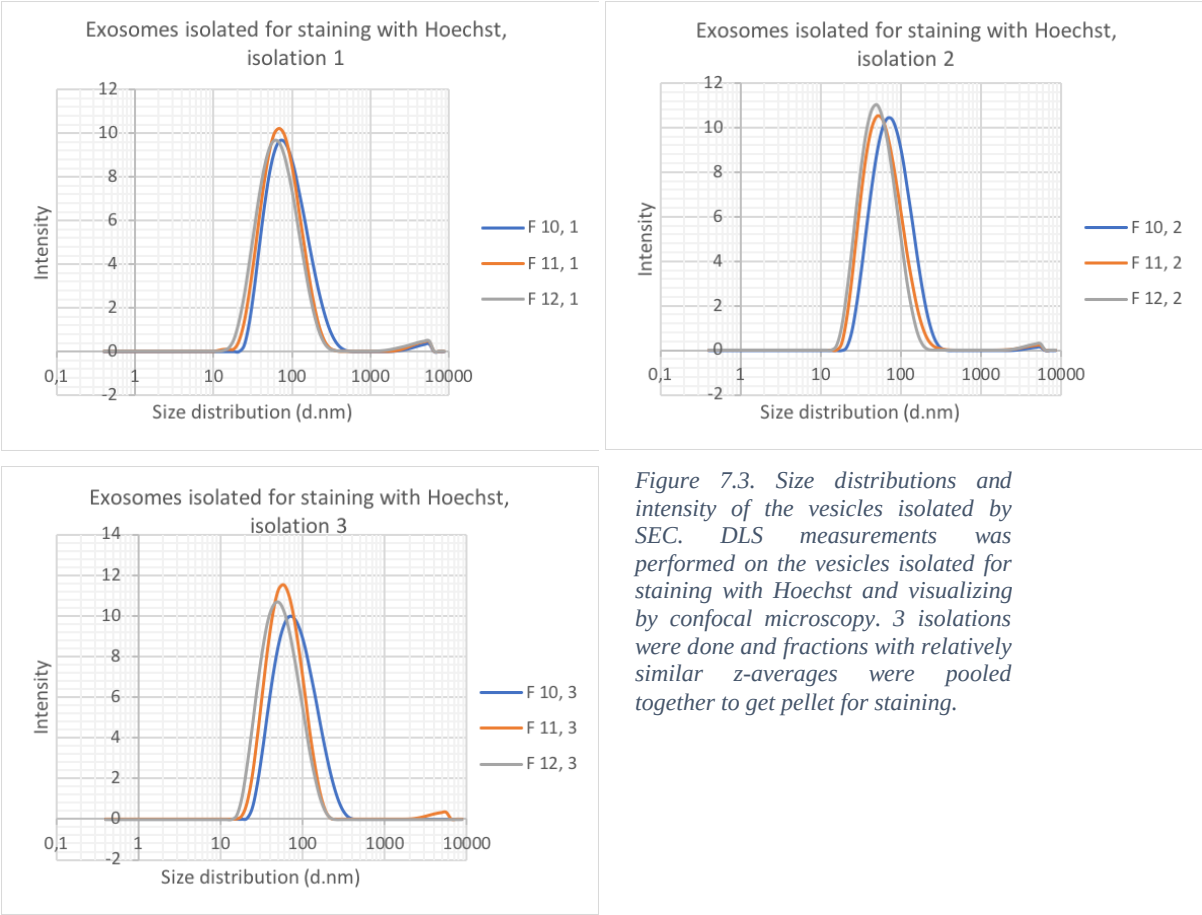

Figure 7.3. Size distributions and intensity of the vesicles isolated by SEC. DLS measurements was performed on the vesicles isolated for staining with Hoechst and visualizing by confocal microscopy. 3 isolations were done and fractions with relatively similar z-averages were pooled together to get pellet for staining.

Table 7.1. Z-averages and PDI-values of the vesicles isolated by SEC for staining with Hoechst and visualizing with confocal microscopy.

Fractions	Z- average (d.nm)	PDI-value
F 10, isolation 1	75.33 ± 0.88	0.2336 ± 0.0109
F 11, isolation 1	64.74 ± 0.23	0.2346 ± 0.0049
F 12, isolation 1	47.11 ± 0.23	0.2493 ± 0.0058
F 10, isolation 2	85.56 ± 0.11	0.2073 ± 0.0089
F 11, isolation 2	66.86 ± 0.09	0.2076 ± 0.0080
F 12, isolation 2	47.11 ± 0.25	0.2053 ± 0.0066
F 10, isolation 3	91.08 ± 0.22	0.2116 ± 0.0046
F 11, isolation 3	54.83 ± 0.12	0.1936 ± 0.0175
F 12, isolation 3	49.63 ± 0.13	0195 ± 0.0043

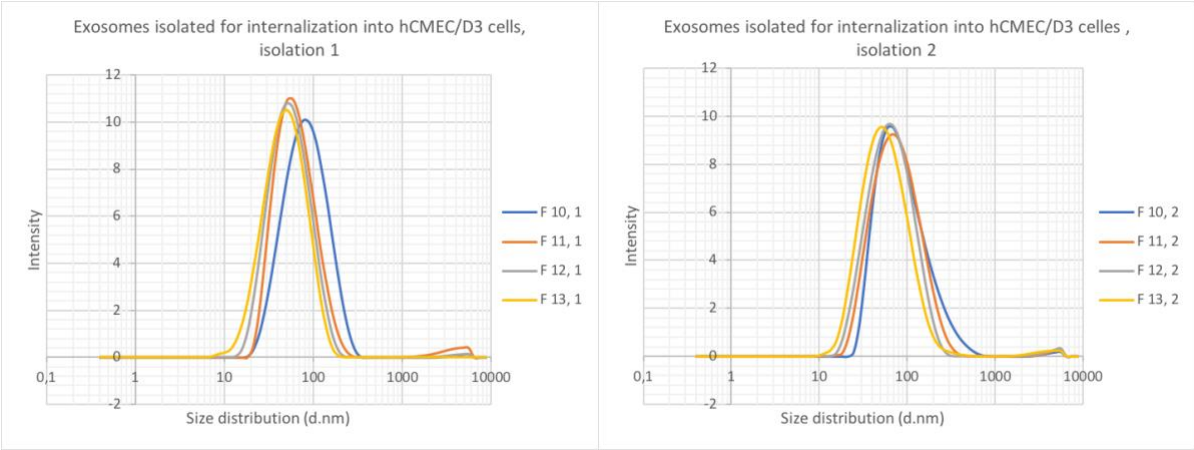

Figure 7.4. Size distribution and intensity of the vesicles isolated by SEC. DLS measurements was performed to the isolations prepared for internalization to hCMEC/D3 cells. Fractions were pooled together two by two to get pellet for staining and adding to the cells.

Table 7.2. Z-averages and PDI-values of the vesicles isolated by SEC for staining with WGA488 and adding to hCMEC/D3 cells.

Fractions	Z- average (d.nm)	PDI-value
F 10, isolation 1	71.75 ± 0.28	0.2186 ± 0.0049
F 11, isolation 1	56.79 ± 0.25	0.217 ± 0.001
F 12, isolation 1	47.80 ± 0.12	0.201 ± 0.00092
F 13, isolation 1	41.5 ± 0.02	0.207 ± 0.0112
F 10, isolation 2	74.62 ± 0.41	0.239 ± 0.0072
F 11, isolation 2	65.05 ± 0.58	0.2366 ± 0.0104
F 12, isolation 2	57.22 ± 0.18	0.2363 ± 0.0048
F 13, isolation 2	48.19 ± 0.43	0.2446 ± 0.0076